# The Formation of Galactic Disks

H.J. Mo, Shude Mao and Simon D.M. White
Max-Planck-Institut für Astrophysik
Karl-Schwarzschild-Strasse 1, 85748 Garching, Germany

## ABSTRACT

We study the population of galactic disks expected in current hierarchical clustering models for structure formation. A rotationally supported disk with exponential surface density profile is assumed to form with a mass and angular momentum which are fixed fractions of those of its surrounding dark halo. We assume that haloes respond adiabatically to disk formation, and that only stable disks can correspond to real systems. With these assumptions the predicted population can match both present-day disks and the damped Ly$\alpha$ absorbers in QSO spectra. Good agreement is found provided: (i) the masses of disks are a few percent of those of their haloes; (ii) the specific angular momenta of disks are similar to those of their haloes; (iii) present-day disks were assembled recently (at $z \leq 1$). In particular, the observed scatter in the size-rotation velocity plane is reproduced, as is the slope and scatter of the Tully-Fisher relation. The zero-point of the TF relation is matched for a stellar mass-to-light ratio of 1 to 2 $h$ in the I-band, consistent with observational values derived from disk dynamics. High redshift disks are predicted to be small and dense, and could plausibly merge together to form the observed population of elliptical galaxies. In many (but not all) currently popular cosmogonies, disks with rotation velocities exceeding 200 km/s can account for a third or more of the observed damped Ly$\alpha$ systems at $z \sim 2.5$. Half of the lines-of-sight to such systems are predicted to intersect the absorber at $r \gtrsim 3\,h^{-1}$kpc and about 10% at $r > 10\,h^{-1}$kpc. The cross-section for absorption is strongly weighted towards disks with large angular momentum and so large size for their mass. The galaxy population associated with damped absorbers should thus be biased towards low surface brightness systems.

*Subject headings:* galaxies: formation - galaxies: structure - galaxies: spiral - cosmology: theory - dark matter

## 1. INTRODUCTION

An important goal of cosmology is to understand how galaxies form. In standard hierarchical models dissipationless dark matter aggregates into larger and larger clumps as gravitational instability amplifies the weak density perturbations produced at early times. Gas associated with such dark haloes cools and condenses within them, eventually forming the galaxies we see today. These two aspects of galaxy formation are currently understood at very different levels. Gravitational processes determine the abundance, the internal structure and kinematics, and the formation paths of the dark haloes, can be simulated in great detail using N-body methods. Well-tested analytic models are now available for describing these properties of the halo population. The growth of the dark haloes is not much affected by the baryonic components, but determines how they are assembled into nonlinear units. Gas cools and collects at the centre of each dark halo until it produces an independent self-gravitating unit which can form stars, heating and enriching the rest of the gas, and perhaps even ejecting it from the halo. These star-formation and feedback processes are not understood in detail and can be modeled or simulated only crudely. Furthermore, as haloes merge to form groups and clusters of galaxies, the cluster members interact and merge both with each other and with the intracluster gas. It will not soon be possible to simulate galaxy formation *ab initio*. At least the star-formation and feedback processes must be put in *ad hoc* based on observations of real galaxies.

In a first exploration of the galaxy population expected in this hierarchical picture White & Rees (1978) calculated the expected luminosity function. The observed characteristic luminosity of galaxies could be reproduced provided (i) that feedback prevents efficient conversion of gas into stars in early objects, and (ii) that merging of galaxies is inefficient as groups and clusters of galaxies build up. The models appeared to overproduce faint galaxies. The formation of galaxy disks within this scheme was studied by Fall & Efstathiou (1980). They showed that if galactic spin is produced by tidal torques acting at early times, then extended massive haloes are necessary if disks as large as those observed are to form by the present day. They also found that plausible initial angular momentum distributions for the gas could lead to near-exponential density profiles for the final disk. More recent analytic work has refined the calculation of global properties of galaxies, for example the distributions of luminosity, colour, morphology and metallicity can all be calculated explicitly in currently popular cosmogonies (e.g. White & Frenk 1991; Kauffmann, White & Guiderdoni 1993; Cole et al 1994; Baugh et al 1997). There has, however, been relatively little work on the internal structure of galaxies. Kauffmann (1996b) studied the accumulation, star-formation and chemical enrichment histories of individual disks, linking them to damped Ly$\alpha$ absorbers at high redshift, but she did not consider the scatter in angular momentum for disks of a given mass and the resulting scatter in their

present-day properties. Dalcanton, Spergel & Summers (1997, hereafter DSS) considered the latter issue in some detail, but did not tie their model explicitly to its cosmogonical context or consider its implications for disk evolution. There have also been surprisingly few well-resolved simulations of galaxy formation from initial conditions which properly reflect the hierarchical model. So far all have failed to produce viable models for observed spirals because excessive transfer of angular momentum from gas to dark matter results in overly small disks (e.g. Navarro & Steinmetz 1997).

In the present paper, we again address the problem of disk formation in hierarchical cosmogonies, formulating a simple model based on four key assumptions: 1) the mass of a disk is some fixed fraction of that of the halo in which it is embedded; 2) the angular momentum of the disk is also a fixed fraction of that of its halo; 3) the disk is a thin centrifugally supported structure with an exponential surface density profile; and 4) only dynamically stable systems can correspond to real galaxy disks. We derive the abundance of haloes in any specific cosmogony from the Press-Schechter formalism, we model their density profiles using the precepts of Navarro, Frenk & White (1996, 1997 hereafter NFW), and we assume their angular momentum distribution to have the near-universal form found in N-body simulations. (See Lacey & Cole 1996 for a summary of how well these analytic models fit simulation results.) Our four assumptions are then sufficient to predict the properties of the disk population, once values are assumed for the mass and angular momentum fractions and the redshift of disk formation. A mass-to-light ratio for the disk stars must also be assumed in order to compare with the luminosities of observed disks. Our assumptions are similar to those of DSS but differ in detail. We calculate many of the same properties as they do, but in addition we address broader issues such as the evolution of disks, the dependence of the disk population on cosmological parameters, and the link with QSO absorption lines.

The outline of our paper is as follows. Section 2 presents our modelling assumptions in detail. To clarify the scaling of disk properties with model parameters, we first treat haloes as singular isothermal spheres and neglect the gravitational effects of the disks. We then consider the more realistic NFW profiles and include the gravitational effects of the disks. In Sections 3 to 5, we describe the predicted properties of present-day disks, we discuss TF relations, we compare high redshift disks with QSO absorption line systems, and we study the effect of a nonrotating central bulge. Finally in Section 6, we discuss other issues related to our model.

## 2. MODELS FOR DISKS IN HIERARCHICAL COSMOGONIES

### 2.1. The cosmogonies

In cold dark matter cosmogonies the evolution of the dark matter is determined by the parameters of the background cosmological model and by the power spectrum of the initial density fluctuations. The relevant cosmological parameters are the Hubble constant $H_0 = 100h\,\mathrm{km\,s^{-1}\,Mpc^{-1}}$, the total matter density $\Omega_0$, the mean density of baryons $\Omega_{b,0}$, and the cosmological constant $\Omega_{\Lambda,0}$. The last three are all expressed in units of the critical density for closure. The power spectrum $P(k)$ is specified in CDM models by an amplitude, conventionally quoted as $\sigma_8$, the *rms* linear overdensity at $z = 0$ in spheres of radius $8h^{-1}$ Mpc, and by a characteristic scale $\Gamma = \Omega_0 h/R$, where $R$ is the current radiation density in units of the standard value corresponding to a $T = 2.73$K black-body photon field and equilibrium abundances of three massless neutrinos. For such cosmogonies the abundance of haloes as a function of mass and redshift can be calculated quite accurately using the Press-Schechter formalism, while their radial density profiles can be calculated as a function of these same variables using the results of Navarro et al (1997). We give some details of how we implement these formalisms in the Appendix.

In the main body of this paper we will compare results for four different CDM cosmogonies. These are specified by particular values of the parameter set $(\Omega_0, \Omega_{\Lambda,0}, h, \Gamma, \sigma_8)$. We do not explicitly need to assume a value for the baryon density $\Omega_{b,0}$, although for consistency we should require $\Omega_{b,0} > m_d\Omega_0$ where $m_d$ is the ratio of disk mass to halo mass adopted (and assumed universal) in our models. This ensures that the disk mass is less than the total initial baryon content of the halo. Our four cosmogonies are:

1. the standard cold dark matter model (SCDM), with $\Omega_0 = 1$, $\Omega_{\Lambda,0} = 0$, $h = 0.5$, $\Gamma = 0.5$, and $\sigma_8 = 0.6$;
2. a COBE-normalized cold dark matter model (CCDM), which has the same parameters as SCDM, except that $\sigma_8 = 1.2$;
3. a $\tau$CDM model, with $\Omega_0 = 1$, $\Omega_{\Lambda,0} = 0$, $h = 0.5$, $\Gamma = 0.2$, and $\sigma_8 = 0.6$; and
4. a $\Lambda$CDM model, with $\Omega_0 = 0.3$, $\Omega_{\Lambda,0} = 0.7$, $h = 0.7$, $\Gamma = 0.2$, and $\sigma_8 = 1.0$.

The $\tau$CDM model could be realised if the $\tau$-neutrino were unstable to decay into other neutrinos and had a mass and lifetime satisfying $m_\tau t_\tau \approx 17$ keV yr (Efstathiou et al 1992). On the relevant scales the power spectrum in this model is quite similar to that of a mixed dark matter (MDM) model with 20 per cent of the critical density in stable neutrinos. The values of $\sigma_8$ adopted for $\tau$CDM and $\Lambda$CDM are consistent both with the observed abundance of rich clusters (see e.g. White, Efstathiou & Frenk 1993; Mo, Jing & White 1996) and with observed anisotropies in the cosmic microwave background (see

e.g. White & Scott 1996), whereas the value for SCDM is consistent only with the cluster normalization and that for CCDM only with the COBE normalization.

### 2.2. Non-self-gravitating disks in isothermal spheres

Many of the properties we predict for galaxy disks can be understood using a very simple model in which dark haloes are treated as singular isothermal spheres and the gravitational effects of the disks themselves are neglected. We will examine the limitations of this rather crude treatment in section 2.3.

For a singular isothermal sphere the density profile is just,

$$\rho(r) = \frac{V_c^2}{4\pi G r^2}, \tag{1}$$

where the circular velocity $V_c$ is independent of radius. Based on the spherical collapse model (Gunn & Gott 1972; Bertschinger 1985; Cole & Lacey 1996), we define the limiting radius of a dark halo to be the radius $r_{200}$ within which the mean mass density is $200\rho_{\rm crit}$, where $\rho_{\rm crit}$ is the critical density for closure at the redshift $z$ when the halo is identified. Thus, the radius and mass of a halo of circular velocity $V_c$ seen at redshift $z$ are

$$r_{200} = \frac{V_c}{10H(z)}; \quad M = \frac{V_c^2 r_{200}}{G} = \frac{V_c^3}{10GH(z)}, \tag{2}$$

where

$$H(z) = H_0 \left[\Omega_{\Lambda,0} + (1-\Omega_{\Lambda,0}-\Omega_0)(1+z)^2 + \Omega_0(1+z)^3\right]^{1/2} \tag{3}$$

is the Hubble constant at redshift $z$. The redshift dependence of halo properties, and so of the disks which form within them, is determined by $H(z)$. In order to understand this dependence better, Figure 1 shows $H(z)/H_0$ as a function of $z$ for open and flat cosmologies with various $\Omega_0$. $H(z)$ increases more rapidly with $z$ in universes with larger $\Omega_0$. For a given $\Omega_0$, the increase is more rapid for an open universe than for a flat universe. At $z \gtrsim 1$, the ratio $H(z)/H_0$ is about twice as large in an Einstein-de Sitter universe as in a flat universe with $\Omega_0 = 0.3$. As a result of this difference, the properties of high redshift disks will depend significantly on $\Omega_0$ and $\Omega_{\Lambda,0}$.

We assume that the mass which settles into the disk is a fixed fraction $m_d$ of the halo mass. The disk mass is then

$$M_d = \frac{m_d V_c^3}{10GH(z)} \approx 1.7\times10^{11} h^{-1} M_\odot \left(\frac{m_d}{0.05}\right)\left(\frac{V_c}{250\,{\rm km\,s^{-1}}}\right)^3 \left[\frac{H(z)}{H_0}\right]^{-1}. \tag{4}$$

Except in Section 5 where we investigate the effects of including a central bulge, we distinguish only halo and disk components, and we assume the disks to be thin, to be in centrifugal balance, and to have exponential surface density profiles,

$$\Sigma(R) = \Sigma_0 \exp\left(-R/R_d\right). \tag{5}$$

Here $R_d$ and $\Sigma_0$ are the disk scalelength and central surface density, and are related to the disk mass through

$$M_d = 2\pi\Sigma_0 R_d^2. \tag{6}$$

If the gravitational effect of the disk is neglected, its rotation curve is flat at the level $V_c$ and its angular momentum is just

$$J_d = 2\pi \int V_c \Sigma(R) R^2 dR = 4\pi\Sigma_0 V_c R_d^3 = 2M_d R_d V_c. \tag{7}$$

We assume this angular momentum to be a fraction $j_d$ of that of the halo, i.e.

$$J_d = j_d J, \tag{8}$$

and we relate $J$ to the spin parameter $\lambda$ of the halo through the definition

$$\lambda = J|E|^{1/2} G^{-1} M^{-5/2}, \tag{9}$$

where $E$ is the total energy of the halo. Equations (7)-(8) then imply that

$$R_d = \frac{\lambda G M^{3/2}}{2V_c|E|^{1/2}} \left(\frac{j_d}{m_d}\right). \tag{10}$$

The total energy of a truncated singular isothermal sphere is easily obtained from the virial theorem by assuming all particles to be on circular orbits:

$$E = -\frac{GM^2}{2r_{200}} = -\frac{MV_c^2}{2}. \tag{11}$$

On inserting this into equation (10) and using equations (2) and (6) we get

$$R_d = \frac{1}{\sqrt{2}} \left(\frac{j_d}{m_d}\right) \lambda r_{200} \approx 8.8 h^{-1}\,\mathrm{kpc} \left(\frac{\lambda}{0.05}\right) \left(\frac{V_c}{250\,\mathrm{km\,s^{-1}}}\right) \left[\frac{H}{H_0}\right]^{-1} \left(\frac{j_d}{m_d}\right), \tag{12}$$

and

$$\Sigma_0 \approx 4.8 \times 10^{22} h\ \mathrm{cm^{-2}} m_{\mathrm{H}} \left(\frac{m_d}{0.05}\right) \left(\frac{\lambda}{0.05}\right)^{-2} \left(\frac{V_c}{250\,\mathrm{km\,s^{-1}}}\right) \left[\frac{H(z)}{H_0}\right] \left(\frac{m_d}{j_d}\right)^2, \tag{13}$$

where $m_{\rm H}$ is the mass of a hydrogen atom. Using equations (5), (12) and (13), we can also obtain the limiting radius, $R_l$, at which the disk surface density drops below some critical hydrogen column $N_l$ (which must be less than $\Sigma_0/m_{\rm H}$):

$$R_l \approx R_d \left\{ 5.5 + \ln \left[ \left( \frac{m_d}{0.05} \right) \left( \frac{m_d}{j_d} \right)^2 \left( \frac{\lambda}{0.05} \right)^{-2} \left( \frac{V_c}{250\,{\rm km\,s^{-1}}} \right) \frac{H(z)}{H_0} \left( \frac{N_l}{2 \times 10^{20} h\ {\rm cm^{-2}}} \right)^{-1} \right] \right\}. \tag{14}$$

This radius depends on $r_{200}$, $\lambda$ and $j_d/m_d$ primarily through the scalelength, $R_d$.

Equations (4) and (12)-(14) give the scalings of disk properties with respect to a variety of physical parameters. These properties are completely determined by the values of $V_c$, $m_d$, $j_d$, $\lambda$ and $H(z)$; other cosmological parameters, such as $z$, $\Omega_0$ and $\Omega_{\Lambda,0}$, affect disks only indirectly through $H(z)$. Since $H(z)$ increases with $z$, disks of given circular velocity are less massive, smaller and have higher surface densities at higher redshifts. At a given redshift, they are larger and less compact in haloes with larger $\lambda$, because they contract less before coming to centrifugal equilibrium. We will approximate the distribution of $\lambda$ by

$$p(\lambda)\,d\lambda = \frac{1}{\sqrt{2\pi}\sigma_\lambda} \exp\left[ -\frac{\ln^2(\lambda/\overline{\lambda})}{2\sigma_\lambda^2} \right] \frac{d\lambda}{\lambda}, \tag{15}$$

where $\overline{\lambda} = 0.05$ and $\sigma_\lambda = 0.5$. This function is a good fit to the N-body results of Warren et al (1992; see also Cole & Lacey 1996; Steinmetz & Bartelmann 1995) except possibly at very small $\lambda$; note that it is narrower than the distribution used by DSS. Since the dependence of $p(\lambda)$ on $M$ and $P(k)$ is weak, we will not consider it further. This model for $p(\lambda)$ is plotted as the dotted curve in Figure 10. The distribution peaks around $\lambda = 0.04$, and has a width of about 0.05. Its 10, 50 and 90 percent points are near $\lambda = 0.025$, 0.05, and 0.1, respectively. Thus we see from equations (12) and (13) that about 10% of disks of given circular velocity will be more than twice the size of the typical disk, and so have less than a quarter the typical surface density, while about 10% will be less than half the typical size, and so have more than four times the typical surface density. (The latter 10% may be unstable – see Section 3.2.)

Disk masses are, of course, directly proportional to $m_d$, the fraction of the halo mass we assume them to contain. For simplicity we will assume this fraction to be the same for all disks, but even in this case it is unclear what value of $m_d$ is appropriate. A plausible upper limit is the baryon fraction of the Universe as a whole, $f_B \equiv \Omega_{b,0}/\Omega_0$, but the efficiency of forming disks could be quite low, implying that $m_d$ could be substantially smaller than $f_B$. Taking a Big Bang nucleosynthesis value for the baryon density, $\Omega_{b,0} = 0.015h^{-2}$ (e.g. Walker et al 1991, but see Turner 1996) gives an upper limit on $m_d$ in the range 0.05 to 0.1 for the cosmological models we consider (see Section 2.1).

If the specific angular momentum of the material which forms the disk is the same as that of the halo, then $j_d/m_d = 1$. This has been the standard assumption in modelling disk formation since the work of Fall & Efstathiou (1980), but it is unclear if it is appropriate, particularly if the the efficiency of disk formation, $m_d/f_B$, is significantly less than unity. Even when this efficiency is high, numerical simulations of spiral galaxy formation have tended to find $j_d/m_d$ values well below unity (e.g. Navarro & White 1994; Navarro & Steinmetz 1997). Equation (12) shows that disk sizes are directly proportional to $j_d/m_d$, and we will find below that values close to unity are required to fit observed spirals. This agrees with the fact that the simulations did indeed produce galaxies with too little angular momentum. Most of our discussion will assume $j_d = m_d$, but we will comment on the effects of changing $m_d$ and $j_d$ independently.

The disk of our own Galaxy has a mass of about $6 \times 10^{10} M_\odot$. Its scalelength and circular velocity (measured at the solar radius, $R_\odot \sim 8\,\mathrm{kpc}$) are $R_d \sim 3.5\,\mathrm{kpc}$ and $V_c \sim 220\,\mathrm{km\,s^{-1}}$ (see Binney & Tremaine 1987, p17). Since the Milky Way appears to be a typical Sbc galaxy, it is interesting to see whether a disk with these parameters is easily accommodated. Equation (4) together with Figure 1 implies that Milky Way-like disks cannot form at $z > 1$ in a universe with $\Omega_0 \sim 1$; for our nucleosynthesis value of $f_B$ the disk mass for $V_c = 220\,\mathrm{km\,s^{-1}}$ is too small even if disks are assumed to form with maximal efficiency. The constraints are weaker for a low-$\Omega_0$ universe, because $f_B$ is larger and $H(z)$ increases less rapidly with $z$. A similar conclusion can be derived from $R_d$. At high redshift the disk scalelength for $V_c = 220\,\mathrm{km\,s^{-1}}$ is too small to match the observed value unless $\lambda \gg 0.05$. Such high values of $\lambda$ are associated with only a small fraction of haloes, and so late formation is required for the bulk of the disk population. As we will see later these constraints become stronger in more realistic models.

If we assume that all disks have the same stellar mass-to-light ratio, $\Upsilon_d \equiv M_d/L_d$ (in solar units), we can cast equation (4) into a form similar to the TF relation:

$$L_d = A \left( \frac{V_c}{250\,\mathrm{km\,s^{-1}}} \right)^\alpha , \tag{16}$$

where $\alpha = 3$ is the slope, and

$$A = 1.7 \times 10^{11} h^{-1} L_\odot \Upsilon_d^{-1} \left( \frac{m_d}{0.05} \right) \left[ \frac{H(z)}{H_0} \right]^{-1} \tag{17}$$

is the 'zero-point'. Notice that $\lambda$ does not appear in these equations. As a result, all the disks assembled at a given time are predicted to lie on a scatter-free TF relation despite the fact that there is substantial scatter in their scale radii and surface densities. The zero-point of this TF relation can, however, depend on the redshift of assembly, being lower

at higher redshifts if the product $\Upsilon(z)H(z)$ is larger. For I-band luminosities the observed value of $\alpha$ is very close to 3 (Willick et al 1995; 1996; Giovanelli et al 1997). Since stellar population synthesis models suggest that $\Upsilon_d$ should vary rather little in this band, we can take this as confirmation of the approximate validity of our assumption that $m_d$ is independent of $V_c$. The zero-point of the observed TF relation corresponds to a value of $A$ of about $5 \times 10^{10} h^{-2} L_\odot$ (Giovanelli et al 1997). Since the expected value of the disk mass-to-light ratio is $\Upsilon_d \approx 1.7h$ (Bottema 1997, see section 3.4), comparison with equation (17) again suggests that late assembly epochs are required; for the appropriate values of $m_d$ the predicted zero-point would be too low if disks formed at high redshift.

The limiting radius $R_l$ which we defined in equation (14) is chosen to be relevant to the damped Ly$\alpha$ absorption lines seen in QSO spectra. Such systems have HI column densities of $N_{\rm HI} \gtrsim 2 \times 10^{20}\,{\rm cm}^{-2}$, comparable to those of present-day galactic disks (see Wolfe 1995 for a review). For given $V_c$ and $\lambda$ disks are smaller at higher redshifts. As a result the cross-section for damped Ly$\alpha$ absorption decreases with $z$. As one can see from equation (14), the limiting radius for damped absorption is roughly $R_l = 5.5 R_d$. For $V_c \sim 200\,{\rm km\,s}^{-1}$ and $\lambda \sim 0.05$, we find $R_l$ between 5 and $10\,h^{-1}$kpc at $z \sim 3$ for $\Omega_0$ between 1 and 0.3. Given the distribution of dark haloes as a function of $\lambda$ and $V_c$, it is clearly possible to calculate the total cross-section for damped absorption along a random sightline, as well as the distributions of $\lambda$, $V_c$, $N_{\rm HI}$ and impact parameter (i.e. the distance between the centre of the absorbing disk and the sightline to the QSO) for the systems actually seen as damped absorbers. We discuss this in detail in section 4.

The model presented in this subsection is limited both because the dark haloes formed by dissipationless hierarchical clustering are only very roughly approximated by singular isothermal spheres, and because the gravitational effects of the disks are often not negligible. Despite this, most of the characteristic properties of this model are retained with only rather minor modifications in the more realistic model which we discuss next.

### 2.3. Self-gravitating disks in haloes with realistic profiles

In a recent series of papers Navarro, Frenk & White (1995; 1996; 1997, hereafter NFW) used high-resolution numerical simulations to show that the equilibrium density profiles of dark matter haloes of all masses in all dissipationless hierarchical clustering cosmogonies can be well fit by the simple formula:

$$\rho(r) = \rho_{\rm crit} \frac{\delta_0}{(r/r_s)(1+r/r_s)^2}, \tag{18}$$

where $r_s$ is a scale radius, and $\delta_0$ is a characteristic overdensity. The logarithmic slope of this profile changes gradually from $-1$ near the centre to $-3$ at large radii. As before (and following NFW) we define the limiting radius of a virialised halo, $r_{200}$, to be the radius within which the mean mass density is $200\rho_{\rm crit}$. The mass within some smaller radius $r$ is then

$$M(r) = 4\pi\rho_{\rm crit}\delta_0 r_s^3 \left[\frac{1}{1+cx} - 1 + \ln(1+cx)\right], \tag{19}$$

where $x \equiv r/r_{200}$, and

$$c \equiv \frac{r_{200}}{r_s} \tag{20}$$

is the halo concentration factor. The total mass of the halo is given by equation (19) with $x = 1$. Using equations (18)-(20), we can obtain a relation between the characteristic overdensity and the halo concentration factor,

$$\delta_0 = \frac{200}{3}\frac{c^3}{\ln(1+c) - c/(1+c)}. \tag{21}$$

We can obtain the total energy of the truncated halo as before by assuming all particles to be on circular orbits, calculating their total kinetic energy, and then using the virial theorem. This yields

$$E = -G\frac{(4\pi\rho_{\rm crit}\delta_0 r_s^3)^2}{2r_s}\left[\frac{1}{2} - \frac{1}{2(1+c)^2} - \frac{\ln(1+c)}{1+c}\right] = -\frac{GM^2}{2r_{200}}f_c, \tag{22}$$

where

$$f_c = \frac{c}{2}\,\frac{1 - 1/(1+c)^2 - 2\ln(1+c)/(1+c)}{[c/(1+c) - \ln(1+c)]^2} \approx \frac{2}{3} + \left(\frac{c}{21.5}\right)^{0.7}. \tag{23}$$

The approximation for $f_c$ given above is accurate to within 1% for the relevant range $5 < c < 30$ (to about 3% for $0 < c < 50$). Comparing equation (22) with equation (11), we see that the total energy for an NFW profile differs from that for an isothermal sphere by the factor, $f_c$, which depends only on the concentration factor.

If the gravitational effects of the disk were negligible, its rotation curve would simply follow the circular velocity curve of the unperturbed halo, $V_c^2(r) = GM(r)/r$. This curve rises to a maximum at $r \approx 2r_s$ and then falls gently at larger radii (see NFW). In fact, disk formation alters the rotation curve not only through the direct gravitational effects of the disk, but also through the contraction it induces in the inner regions of the dark halo. We analyse this effect by assuming that the halo responds adiabatically to the slow assembly of the disk, and that it remains spherical as it contracts; the angular momentum of individual dark matter particles is then conserved and a particle which is initially at mean radius, $r_i$, ends up at mean radius, $r$, where

$$GM_f(r)r = GM(r_i)r_i. \tag{24}$$

In this formula $M(r_i)$ is given by the NFW profile (19) and $M_f(r)$ is the total final mass within $r$. [See Barnes & White (1984) for a test of this adiabatic model.] The final mass is the sum of the dark matter mass inside the initial radius $r_i$ and the mass contributed by the exponential disk. Hence

$$M_f(r) = M_d(r) + M(r_i)(1 - m_d), \tag{25}$$

where, as before, $m_d$, is the fraction of the total has in the disk, and

$$M_d(r) = M_d \left[1 - \left(1 + \frac{r}{R_d}\right) e^{-r/R_d}\right]. \tag{26}$$

Here we implicitly assume that the baryons initially had the same density profile as the dark matter, and those which do not end up in the disk remain distributed in the same way as the dark matter. For a given rotation curve, $V_c(R)$, the total angular momentum of the disk can be written as

$$J_d = \int_0^{r_{200}} V_c(R) R \Sigma(R) 2\pi R dR = M_d R_d V_{200} \int_0^{r_{200}/R_d} e^{-u} u^2 \frac{V_c(R_d u)}{V_{200}} du, \tag{27}$$

where $V_{200} \equiv V_c(r_{200})$ is unaffected by disk formation. In practice we can set the upper limit of integration to infinity because the disk surface density drops exponentially and $r_{200} \gg R_d$. Substituting equation (22) into equation (9) and writing $J_d = j_d J$, we can use the argument of Section 2.2 to obtain

$$R_d = \frac{1}{\sqrt{2}} \left(\frac{j_d}{m_d}\right) \lambda r_{200} f_c^{-1/2} f_R(\lambda, c, m_d, j_d) \tag{28}$$

where

$$f_R(\lambda, c, m_d, j_d) = 2 \left[\int_0^\infty e^{-u} u^2 \, \frac{V_c(R_d u)}{V_{200}} \, du\right]^{-1}. \tag{29}$$

Comparing equation (28) with equation (12) we see two effects that cause the disk scalelength to differ from that in a singular isothermal sphere; the factor $f_c^{-1/2}$ comes from the change in total energy resulting from the different density profile, while the factor $f_R(\lambda, c, m_d, j_d)$ is due both to the different density profile and to the gravitational effects of the disk.

The rotation velocity $V_c(r)$ is a sum in quadrature of contributions from the disk and from the dark matter:

$$V_c^2(r) = V_{c,d}^2(r) + V_{c,DM}^2(r), \tag{30}$$

where

$$V_{c,DM}^2(r) = G \left[M_f(r) - M_d(r)\right] / r, \tag{31}$$

and $V_{c,d}(r)$ is the rotation curve which would be produced by the exponential disk alone. Note that when calculating the latter quantity the flattened geometry of the disk has to be taken into account (Binney & Tremaine 1987, p77). For a given set of parameters, $V_{200}$, $c$, $\lambda$, $m_d$ and $j_d$, equations (25), (26), (28) and (30) must be solved by iteration to yield the scale length, $R_d$, and the rotation curve, $V_c(R)$. For example, we can start with a guess for $R_d$ by setting $f_R = 1$ in equation (28). We can then obtain $M_d(r)$ from equation (26). Substituting this into equation (25) and using equation (24), we can solve for $r_i$ as a function of $r$ and so obtain $M_f(r)$ from equation (25). With this and with $V^2_{c,d}(r)$ calculated for the assumed $R_d$, we can get the disk rotation curve from equations (30) and (31). Inserting this into equation (29) and using equation (28) we then obtain a new value for $R_d$. In practice this iteration converges rapidly, so that accurate values for both $R_d$ and $V_c(r)$ are easily obtained.

It is useful to have a fitting formula for $f_R$ which allows this iterative procedure to be avoided. We find that the following expression has sufficient accuracy:

$$f_R \approx \left(\frac{\lambda'}{0.1}\right)^{-0.06+2.71m_d+0.0047/\lambda'} (1-3m_d+5.2m_d^2)(1-0.019c+0.00025c^2+0.52/c), \quad (32)$$

where $\lambda' \equiv (j_d/m_d)\lambda$. We will see in Section 3.1 that the rotation curves predicted by our procedure typically reach a maximum near $3R_d$ and in much of the discussion which follows we will use the value at this point to characterise their amplitude. As a result, it is also useful to have a fitting formula for the dimensionless coefficient $f_V(\lambda, c, m_d, j_d)$ in

$$V_c(3R_d) = \left(\frac{GM}{r_{200}}\right)^{1/2} f_V = V_{200} f_V. \quad (33)$$

We find

$$f_V \approx \left(\frac{\lambda'}{0.1}\right)^{-2.67m_d-0.0038/\lambda'+0.2\lambda'} (1+4.35m_d-3.76m_d^2)\frac{1+0.057c-0.00034c^2-1.54/c}{[-c/(1+c)+\ln(1+c)]^{1/2}}. \quad (34)$$

The approximations in (32) and (34) are accurate to within 15% for $5 < c < 30$, $0.02 < \lambda' < 0.2$ and $0.02 < m_d < 0.2$.

## 3. THE SYSTEMATIC PROPERTIES OF DISKS

### 3.1. Rotation curves

According to the model set out in Section 2.3 the shape of a disk's rotation curve depends on the concentration of its halo, $c$, on the fraction of the halo mass which it

contains, $m_d$, and on its angular momentum as specified by the parameter combination $\lambda' = (j_d/m_d)\lambda$. For given values of these three parameters the amplitude of the rotation curve and its radial scale are set by any single scale parameter, either for the halo ($M$, $r_{200}$, or $V_{200}$) or for the disk ($M_d$, $R_d$, or $\Sigma_0$). Figure 2 shows examples chosen to illustrate how changes in $m_d$, $\lambda'$ and $c$ affect the shape of the rotation curve of a disk of fixed mass. Curves for other disk masses can be obtained simply by scaling both axes by $M_d^{1/3}$. In all cases the rotation curves are flat at radii larger than a few disk scalelengths. At smaller radii the shape of the curves depends strongly on the spin parameter. For small values of $\lambda'$ the disk is more compact, and its self-gravity is more important. The rotation velocity then increases rapidly near the centre to a peak near $R \sim 3R_d$, thereafter dropping gradually towards a plateau at larger radii. For large $\lambda'$, the disk is much more extended and its self-gravity is negligible. The rotation velocity then increases slowly with radius in the inner regions.

Since the surface density of a disk is roughly proportional to $(\lambda')^{-2}$, these results imply a correlation between disk surface brightness and rotation curve shape which is very reminiscent of the observational trends pointed out by Casertano & van Gorkom (1991). Our predicted rotation curves also become more peaked at small radii for larger values of $m_d$, again because of the larger gravitational effect of the disk. Rotation curves as peaked as that shown in the lower left panel of Figure 2 are not observed. As we will discuss below, this is probably because such disks are violently unstable. Halo concentration affects rotation curves in the obvious way; more strongly peaked curves are found in more concentrated haloes. Combining these trends we conclude that slowly increasing rotation curves are expected for low-mass disks in haloes with large $\lambda'$ and small $c$. Since $c$ is smaller for more massive haloes (see NFW), we would predict slowly rising rotation curves to occur preferentially in giant galaxies. In fact, the opposite is observed. This is almost certainly a result of the greater influence of the bulge in giant systems. A final trend which is clear from Figure 2 is that at fixed disk mass more strongly peaked curves have larger maximum rotation velocities. A similar trend can be seen in the observational data (e.g. Persic and Salucci 1991).

### 3.2. Disk instability

The modelling of the last two sections can lead to disks with a very wide range of properties. Not all of these disks, however, are guaranteed to be physically realisable. In particular, those in which the self-gravity of the disk is dominant are likely to be dynamically unstable to the formation of a bar. There is an extensive literature on such

bar instabilities [see Christodoulou, Shlosman & Tohline (1995) and references therein]. For our purposes the most relevant study is that of Efstathiou, Lake & Negroponte (1982) who used N-body techniques to investigate global instabilities of exponential disks embedded in a variety of haloes. They found the onset of the bar instability for stellar disks to be characterised by the criterion,

$$\epsilon_{\rm m} \equiv \frac{V_{\rm max}}{(GM_d/R_d)^{1/2}} \lesssim 1.1, \tag{35}$$

where $V_{\rm max}$ is the maximum rotation velocity of the disk. The appropriate instability threshold for gas disks is lower, $\epsilon_{\rm m} \lesssim 0.9$, as discussed in Christodoulou et al (1995). In our model,

$$\epsilon_{\rm m} \approx \frac{1}{2^{1/4}} \left(\frac{\lambda'}{m_d}\right)^{1/2} f_c^{-1/4} f_R^{1/2} f_V. \tag{36}$$

Thus, disks are stable if

$$\lambda' \gtrsim \lambda'_{\rm crit} = \sqrt{2}\epsilon^2_{\rm m,crit} m_d f_c^{1/2} f_R^{-1} f_V^{-2}, \tag{37}$$

where $\epsilon_{\rm m,crit} \approx 1$ is the critical value of $\epsilon_{\rm m}$ for disk stability. If the effect of disk self-gravity on $R_d$ and $V_c$ is weak, then $\lambda'_{\rm crit} \sim m_d$. Figure 3 shows $\lambda'_{\rm crit}$ as a function of $m_d$ for our NFW models. Results are shown for $\epsilon_{\rm m,crit} = 0.8$, 1, and 1.2, in order to bracket the critical values of $\epsilon_{\rm m}$ discussed above. In practice we will normally adopt $\epsilon_{\rm m,crit} = 1$ as a fiducial value. The dependence of $\lambda'_{\rm crit}$ on halo concentration is weak, because for a given $m_d$, the dependences of $V_{\rm max}$ and $R_d$ on $c$ are opposite. Since halo mass and assembly time affect $\lambda'_{\rm crit}$ only through $c$, we expect disk stability to be almost independent of these parameters. As one can see from Figure 3, it is a useful rough approximation to take $\lambda' > m_d$ as the condition for stability. Thus in Figure 2 the top two disks are marginally stable, the lower left disk is strongly unstable and the lower right disk is stable.

Disk galaxies are common and appear to be stable. If we take account of the expected distribution of $\lambda$ (equation 15) and the likelihood that $j_d \leq m_d$, then the results in Figure 3 suggest that $m_d$ values of 0.05 or less will be needed to ensure that most haloes host stable disks rather than the descendants of unstable disks.

### 3.3. Disk scalelengths and formation times

For a given cosmogony our assumptions determine the joint distribution of disk size and rotation speed once values are adopted for the mass and angular momentum fractions, $m_d$ and $j_d$, and for the disk formation redshift. This distribution can be compared directly

with observation provided our size measure, $R_d$, can be identified with the exponential scalelength of observed luminosity profiles. This seems reasonable since there is no evidence that the mass-to-light ratio of the stellar populations in real disks are a strong function of radius. In our simplified model the disk "formation redshift" is just the time at which the arguments of Section 2 are applied. We make no attempt to follow the actual formation and evolution of disks, and we assume that all disks form at the same time. This formation redshift should be interpreted as the epoch when the material actually observed was assembled into a single virialised object.

Figure 4 compares predicted distributions of $R_d$ as a function of $V_c$ with observational data for a large sample of nearby spirals. The four panels give predictions for formation redshifts of 0 and 1, and for two different cosmogonies, SCDM and ΛCDM; predictions for CCDM and $\tau$CDM are similar to those for SCDM. As a characteristic measure of rotation speed for our model galaxies we use the value of $V_c$ at $3R_d$. As discussed in §2.3 this is always close to the maximum of the rotation curve. The solid line in each panel is the $R_d$-$V_c$ relation for *critical* disks (i.e. those with $\lambda' = \lambda'_{\rm crit}$) for the case $m_d = 0.05$; stable disks must lie above this line. Since $\lambda'_{\rm crit} \approx 0.05$ in this case, and since, in general, we expect $j_d \leq m_d$, implying $\lambda' \leq \lambda$, at most half of all dark haloes will contain stable disks for $m_d \geq 0.05$ (see the discussion around equation 15). The short-dashed line in each panel is the corresponding critical line for $m_d = 0.025$. In this case about 90 percent of the dark haloes can host stable disks under the optimistic assumption that $j_d = m_d$. The critical lines would be even lower if $m_d < 0.025$, but values of $\lambda$ below 0.025 are rare, and so such compact disks will not be abundant unless $j_d$ is often substantially smaller than $m_d$. Finally, the long-dashed lines in Figure 4 show $R_d$-$V_c$ relations for $m_d = j_d = 0.05$ and $\lambda = 0.1$. For these parameters disk self-gravity is negligible and the line is almost unaltered for $m_d = j_d = 0.025$. Fewer than 10 percent of the dark haloes have $\lambda \geq 0.1$ in the $\lambda$-distribution of equation (15). Thus for $j_d \leq m_d$ very few disks are expected to lie above these long-dashed lines. The slopes and relative amplitudes of all the theoretical lines in Figure 4 can easily be understood from the scalings in equation (12).

The data points in Figure 4 are the observational results of Courteau and coworkers (Courteau 1996; 1997; Broeils & Courteau 1996) for *present-day* normal spirals. For a formation redshift of zero, the observed distribution lies comfortably below the long dashed lines and above the short dashed lines in both cosmologies. A significant fraction of the disks lie below the solid lines, particularly for ΛCDM, suggesting that these disks must have $m_d < 0.05$ in order to be stable. For this formation redshift it seems relatively easy to reproduce the observed distribution in both cosmogonies. For a formation redshift of 1, in contrast, the observed points clearly lie too high relative to the predictions of the SCDM model (and similarly for CCDM and $\tau$CDM). Observed disks are too big to have formed

at $z \sim 1$ in a high density universe, unless there is some way for $j_d$ to be substantially larger than $m_d$. The observed points also lie rather high for $z = 1$ in ΛCDM, but here the discrepancy is marginal provided that $j_d \sim m_d$ is indeed a realistic expectation. It is clear that substantial transfer of angular momentum from baryons to dark matter, resulting in $j_d \ll m_d$, would lead to unacceptably small disks for any assembly redshift in all of the cosmogonies we consider. Note that although the observed disks of Figure 4 apparently formed late, this does not mean that disks were not present in large numbers at high redshift; early disks should, however, be significantly smaller than present-day objects of the same $V_c$.

For the cosmogonies considered here, the comoving number density of galaxy-sized haloes is expected to peak at $z \sim 1$ and then to decline gradually at lower redshift. The peak density is comparable to the number density of galaxies observed today. Thus, as can be seen explicitly from more detailed semi-analytic modelling (e.g. Kauffmann et al 1993) these models do indeed predict enough haloes to house the observed population of disks. Late formation thus appears viable both in terms of the structural properties and the abundance of disks in CDM-like models.

### 3.4. Disk surface densities

For a given cosmogony the distributions of $M$ (the halo mass) and $\lambda$ are known as a function of redshift [see equations (A5) and (15)], and furthermore the halo concentration factor, $c$, can be calculated from $M$ and $z$ (we neglect any scatter in $c$, see the Appendix). For any particular formation redshift, we can therefore generate Monte-Carlo samples of the halo distribution in the $M$-$\lambda$ plane, and, using specific values for $m_d$ and $j_d$, transform these into Monte-Carlo samplings of the disk population. Figure 5 shows the distribution of disks in the $V_c$-$\Sigma_0$ plane for SCDM with $m_d = 0.025$, 0.5 and 0.1, $j_d = m_d$ and a formation redshift of zero. Unstable disks with $\epsilon_{\rm m} < 1$ are excluded. The instability criterion leads to an upper cutoff in the central surface luminosity density $\Sigma_0$. For the simple isothermal sphere model of §2.2 this upper cutoff can be written as

$$\Sigma_{\rm crit} \propto \frac{m_d}{(\lambda'_{\rm crit})^2} H(z) V_c \propto \frac{V_c}{\lambda'_{\rm crit}} H(z) \propto \frac{V_c}{m_d} H(z), \tag{38}$$

where we have used $\lambda'_{\rm crit} \approx m_d$ (see equation 37). Thus $\Sigma_{\rm crit}$ is larger for higher $z$, for higher $V_c$ and for lower $m_d$. The last two dependences are clearly seen in Figure 5.

To compare the distributions of Figure 5 with real data we need to assume a stellar mass-to-light ratio for the disks. Throughout this article we will use the values found

for high surface brightness disks by Bottema (1997). From disk dynamics, he inferred $\Upsilon_B = (1.79 \pm 0.48)$ for $h = 0.75$. Since $B - I = 1.7$ for a typical disk galaxy (McGaugh & de Blok 1996), and $(B - I)_\odot = 1.33$, we obtain $\Upsilon_I = (1.7 \pm 0.5)h$. Solid squares in Figure 5 correspond to median values for the Courteau data in Figure 4. We have converted from $V_c$ to $L_I$ using the Tully-Fisher relation of Giovanelli et al (1997; equation 39), and from $L_I$ to $\Sigma_0$ using equation (6) and $\Upsilon_I = 1.7h$. Error bars join the upper and lower 10% points of the distribution in each $V_c$ bin. The typical central surface brightnesses found in this way are similar to the "standard" value advocated by Freeman (1970). For $m_d = 0.05$, the median central surface density for disks at $z = 0$ in SCDM appears to be about a factor of 2 too faint compared with the observed value. However, this discrepancy should not be over-interpreted since low surface brightness galaxies are probably underrepresented in Courteau's sample. In addition, the model prediction has substantial uncertainties. For a given $V_c$, the predicted disk surface density is proportional to $H(z)$, and so a formation redshift of 0.5 would increase the predictions by a factor of 1.8. Furthermore, the upper cutoff of the disk surface density distribution depends sensitively on the value of $\epsilon_{\rm m,crit}$ (cf. equation 35). For a given $m_d$, $\Sigma_{\rm cr} \propto \epsilon_{\rm m,crit}^{-4}$; a 20% decrease in $\epsilon_{\rm m,crit}$ would thus increase the upper cutoff on $\Sigma_0$ by a factor of two.

Despite these uncertainties, Figure 5 suggests that $m_d \lesssim 0.05$ is preferred. Notice that this conclusion is independent of the $R_d$-$V_c$ analysis of the last section which suggested similar values for $m_d$. It is interesting that the abundance of both high and low surface density galaxies is predicted to increase as $m_d$ decreases. This is a consequence of the wider range of $\lambda$ values which produce stable disks when $m_d$ is small. There is currently considerable debate about the relative abundance of low-surface-brightness (LSB) galaxies. Our results confirm those of Dalcanton et al (1997); hierarchical models can relatively easily produce a spread which appears broad enough to be consistent with the observations. We note that an additional uncertainty in any detailed comparison comes from the fact that the star formation efficiency in disks may well vary strongly as a function of surface density. This would further complicate the conversion between disk mass and disk light.

### 3.5. Tully-Fisher relations

In one of the most complete recent studies of the Tully-Fisher relation for nearby galaxies Giovanelli et al (1997) put together a homogeneous set of HI velocity profiles and I-band photometry for a set of 555 spiral galaxies in 24 clusters. By careful adjustment of the relative zero-points of the different clusters they derived a TF relation in the (Cousin)

I-band,

$$\mathcal{M}_I - 5\log h = -(21.00 \pm 0.02) - (7.68 \pm 0.13)(\log W - 2.5), \tag{39}$$

where $W$ is the inclination-corrected width of the HI line profile, and, to a good approximation, is twice the maximum rotation velocity. When comparing with our models we will assume $W = 2V_c(3R_d)$ ( see §2.3). Giovanelli et al find a mean scatter around this relation of 0.35 magnitudes, but point out that the scatter is actually magnitude-dependent; it increases significantly with decreasing velocity width. A nearly identical Tully-Fisher relation was derived independently by Shanks (1997), but the zero-point of the TF relation in Willick et al (1996) is fainter by about 0.5 mag.

In order to derive luminosities for the disks in our models we need to specify their stellar mass-to-light ratio. Unfortunately, the appropriate value for this quantity is quite uncertain; here we will again use the value $\Upsilon_I = 1.7h$ which Bottema (1997) derived for the disks of high surface brightness spirals. For a given mass-to-light ratio, the magnitude of a disk galaxy can be calculated as

$$\mathcal{M}_I = \mathcal{M}_{\odot,I} - 2.5\log\frac{L_I}{L_{\odot,I}} = 4.15 - 2.5\log\frac{M_d}{M_\odot} + 2.5\log(\Upsilon_I), \tag{40}$$

where we have used $\mathcal{M}_{\odot,V} = 4.83$, and $(V-I)_\odot = 0.68$ (Bessel 1979, Table II). Note that in the observed TF relation $\mathcal{M}_I$ is the total absolute magnitude of the galaxy, whereas for our models we are estimating the absolute magnitude of the disk alone; we are therefore implicitly assuming that the bulge luminosity can be neglected for the galaxies under consideration (but see §5 below).

With these assumptions, we can generate a Monte-Carlo disk catalogue, as in §3.4, and plot $\mathcal{M}_I$ versus $V_c(3R_d)$ ($\approx W/2$). Figure 6 shows such plots for stable disks with a formation redshift of $z = 0$ in SCDM and ΛCDM. Here we assume $m_d = j_d = 0.05$. For each cosmogony, the three panels show results for three choices of $\epsilon_{\rm m,crit}$, the critical value of $\epsilon_{\rm m}$ for disk instability (equations 35 to 37). As one can see, the plots are similar in all cases. The zero point for the SCDM model is lower than that for the ΛCDM model for the reasons to be discussed in more detail in section 3.5.3. The scatter is slightly larger for smaller values of $\epsilon_{\rm m,crit}$, because disks are then stable for smaller $\lambda$ values where disk self-gravity is more important. By fitting plots such as these we can clearly derive TF relations for our models, and so can compare their slope, scatter and zero-point with those of the observed Tully-Fisher relation.

### *3.5.1. Tully-Fisher slopes*

We begin by considering the slopes of the model relations. The solid lines in Figure 6 are the linear regressions of $\mathcal{M}_I$ on $V_c$ for each Monte-Carlo sample of simulated data. It is clear that in all cases the slope is close to $\alpha = 3$ (where $\alpha$ is defined in equation 16), and is consistent with the observed value of Giovanelli et al which we indicate with a dashed line. Although there is clearly very good agreement, it is important to realise that this is a consequence of choosing to compare with the observed I-band data. In fact, the observed slope is quite dependent on the photometric band used. For example, in the B-band it is about $\alpha = 2.5$ (Strauss & Willick 1995 and references therein). This difference arises because the colours of disk galaxies vary systematically with their luminosity; fainter galaxies show proportionately more star formation and are bluer. Stellar population models suggest that the stellar mass-to-light ratios of disks must vary quite strongly with luminosity in the B-band (being smaller for the fainter, bluer galaxies) but could plausibly be constant at I. For this reason the I-band TF relation does indeed appear to be the most appropriate one to compare with our models.

In the models the slight deviation of the slope from $\alpha = 3$ is caused by the fact that massive haloes are less concentrated than low-mass haloes. To see this, we recall NFW's discovery that the concentration factor of a halo is determined by its formation time $z_f$; massive haloes form later and so are less concentrated (see the Appendix). Since the value of $f$ in equation (A10) is small, we have $\delta_{z_f} - \delta_c \propto \sigma(fM)$. For galactic haloes, $\sigma(fM) \gg 1$ in all the cosmogonies considered here, and so $\delta_{z_f} - \delta_c \approx \delta_{z_f} \propto (1 + z_f)$. Writing the *rms* mass fluctuation defined in equation (A4) as $\sigma^2(r_0) \propto r_0^{-(3+n_{\rm eff})}$, we have $(1 + z_f) \propto (fM)^{-(3+n_{\rm eff})/6}$. On galactic scales, the effective power index $n_{\rm eff} \sim -2$ for our CDM models, so that more massive haloes have lower values of $z_f$, and so also of $c$. The value of $\alpha$ is slightly larger for SCDM, because $n_{\rm eff}$ is slightly larger in this case. As shown by Navarro et al (1997), if $n_{\rm eff}$ differs substantially from $-2$, then $\alpha$ can be very different from 3. The effect of changing the *amplitude* of the fluctuation spectrum is negligible, and the slope is also insensitive to changes in $m_d$, $j_d$, and the formation redshift of disks, provided none of these parameters varies with $V_c$. The observed slope of the TF relation is thus a generic prediction of hierarchical models with CDM-like fluctuation spectra.

### *3.5.2. Tully-Fisher scatter*

The observed scatter in the TF relation is quite small; Giovanelli et al (1997) quote 0.35 magnitudes as an overall measure of scatter, while Willick et al (1995,1996) find 0.4

magnitudes to be typical. It is clear from Figure 6 that we do indeed predict a small scatter, but it is important to understand why. In the model of Section 2.2 the gravitational effect of disks is neglected, all haloes of the same mass have identical singular isothermal density profiles, and all disks have the same $m_d$ and $\Upsilon_d$. With these assumptions the TF relation has no scatter even though the broad $\lambda$-distribution leads to a wide range of disk sizes and surface brightnesses. In the more realistic model of Section 2.3, scatter in the TF relation can arise from two effects. For given disk and halo masses, the maximum rotation is larger for more compact disks, i.e. for those residing in more slowly spinning haloes. As a result, the scatter in the $\lambda$-distribution of haloes translates into a scatter about the predicted TF relation. This is the source of scatter in Figure 6; this scatter remains small because the stability requirement eliminates the most compact systems. In addition, even for given $M_d$, $M$ and $\lambda$, the disk rotation velocity will be larger in more concentrated haloes. Thus any scatter in $c$ will produce scatter in the TF relation. We now examine the consequences of these two effects in detail.

The solid curves in Figure 7 show the scatter about the mean model TF relations as a function of $\lambda_l$, an assumed lower limit on $\lambda$ for the haloes allowed to contribute observable disks. For given $m_d$, this function is sensitive neither to cosmological parameters nor to the redshift of disk formation. The scatter increases as haloes with lower values of $\lambda$ are included, because disk self-gravity becomes important for such systems. It increases with $m_d$, because the contribution of a disk to the rotation velocity is then larger at fixed $\lambda$. It is clear that the predicted scatter can be made sufficiently small, provided disks with large $m_d$ and small $\lambda$ are excluded. The arrows next to each curve in Figure 7 show the smallest value of $\lambda$ for which disks with the given value of $m_d$ are stable (here we conservatively require $\epsilon_{\rm m} > 0.8$). It is clear that the predicted scatter is smaller than observed if $m_d \gtrsim 0.025$. For even smaller $m_d$, a larger range of $\lambda$ is allowed for stable disks, leading to a larger scatter. This is a consequence of the deviation between the NFW profile and an isothermal sphere. Since only about 10 percent of haloes have $\lambda < 0.025$, the increased scatter in this case is due to a relatively small number of compact outliers.

The distribution of the halo concentration factor at fixed mass is poorly known. In the simulations of NFW, the *rms* scatter in $c$ is $\Delta c/c \approx 25\%$. To demonstrate the effect of such scatter on the predicted TF relation, the dashed curves in Figure 7 show the predicted scatter if we assume a 25% *rms* uncertainty in the concentration parameter of haloes of a given mass. (Note: NFW show that the scatter in $c$ is uncorrelated with $\lambda$.) If this variability in halo profiles is indeed realistic, it is clear from Figure 7 that it adds relatively little scatter to the TF relation. As NFW point out, this is in conflict with the conclusions of Eisenstein & Loeb (1996) from an analytic assessment of the expected variation in halo profiles. In summary, the analysis of this section suggests that it may not be difficult

for hierarchical models to produce a disk population with Tully-Fisher scatter within the observed limits. We note, however, that we have not included the bulge contribution to the luminosity of the galaxies or possible variations in $\Upsilon_d$. Both presumably act to increase the TF scatter.

### *3.5.3. The Tully-Fisher zero-point*

The zero-point of the predicted TF relation depends weakly on the distribution of $\lambda$ and on our stability requirement. On the other hand, it depends strongly on $m_d$, the fraction of the halo mass in disks, on $\Upsilon_d$, the stellar mass-to-light ratio of the disks, and on $z$, the redshift at which disk material is assembled within a single dark halo. Figure 8 shows the values of $\Upsilon_d h^{-1}$ required to reproduce the observed zero-point of the $I$-band TF relation (equation 39) as a function of $m_d$. Zero-points are calculated for stable disks with $\epsilon_{\rm m} > 1$ (the results are very similar for $\epsilon_{\rm m} > 0.8$ or $> 1.2$). In all cases the required mass-to-light ratio is approximately proportional to $m_d$. The three arrows in each panel show the values of $m_d$ at which 10%, 50% and 90% of the haloes can host stable disks.

Stable disk galaxies are common and there are no obvious observational counterparts for a large number of "failed" unstable disks. The $z = 0$ lines in this figure thus suggest $\Upsilon_d < 1h$ in the $I$-band for the CCDM model, whereas for SCDM, ΛCDM and $\tau$CDM the upper limit gets progressively weaker. This trend is a consequence of the steadily decreasing concentration of haloes of given mass along this sequence, which results in a corresponding decrease in the maximum rotation velocity. The same trend can be seen quite clearly in Figure 6. The maximum allowed mass-to-light ratio is even smaller for higher assembly redshifts, because disks are then less massive for a given $V_c$. The horizontal dotted lines in Figure 8 bracket the $\pm 1\sigma$ range derived by Bottema (1997) from his analysis of the dynamics of observed disks. This range takes account of the fact that some (dim) disks may have as much as half of their mass in gas. As one can see, in order to reproduce the Tully-Fisher zero-point with $\Upsilon_I$ in the allowed range, normal disks could form at high $z$ only if $m_d$ is large, while for low formation redshifts $m_d < 0.05$ is possible. For $m_d > 0.05$ most haloes *cannot* host stable disks, so we infer that normal spiral disks must form late with an effective assembly redshift close to zero. A reasonable zero-point then requires $m_d \gtrsim 0.03$, in good agreement with the values obtained above from the observed sizes and surface brightnesses of disks. Finally we note that because disk self-gravity is less important for larger values of $\lambda$, somewhat higher mass-to-light ratios are needed if LSB galaxies are to fit on the same Tully-Fisher relation as normal spirals.

## 4. HIGH REDSHIFT DISKS AND DAMPED LYMAN ALPHA SYSTEMS

Damped Ly$\alpha$ absorption systems (DLS), corresponding to absorbing clouds with a neutral column density, $N_{\rm HI} \gtrsim 2 \times 10^{20}\,{\rm cm}^{-2}$, are seen in the spectra of many high redshift QSOs. Their abundance varies very roughly as $n(z) \sim 0.03(1+z)^{1.5}$ over the redshift range $1.5 < z < 4$, and their total HI content is a few tenths of a percent of the critical density, about the same the total mass in stars in the local universe (see e.g. Storrie-Lombardi et al 1996). Over the last decade Wolfe and his collaborators have used a wide range of observational indicators, most recently the velocity structure in the associated metal lines, to argue that these systems correspond to large equilibrium disks with $V_c \gtrsim 200\,{\rm km\,s}^{-1}$, the extended and gas-rich progenitors of present-day spirals (Wolfe et al 1986; Lanzetta, Wolfe & Turnshek 1995; Wolfe 1995; Prochaska & Wolfe 1997, but see Jedamzik & Prochaska ). Early theoretical studies showed that the total HI content of these systems can be reproduced in some but not all hierarchical cosmologies, provided systems with circular velocities well below 200 km/s are allowed to contribute (Mo & Miralda-Escudé 1994; Kauffmann & Charlot 1994; Ma & Bertschinger 1994; Klypin et al 1995). A detailed study of the standard CDM cosmology by Kauffmann (1996b) concluded that disks in all haloes down to $V_c \sim 50$ km/s must contribute, once a realistic model for star formation is included. Numerical simulations by Gardner et al (1997) led these authors to a similar conclusion, while higher resolution simulations by Haehnelt, Steinmetz & Rauch (1997) showed that the kinematic data of Prochaska & Wolfe (1997) can be reproduced by nonequilibrium disks in low mass haloes and so do not *require* large $V_c$. These simulations did not include star formation. The cross-sections they imply should be viewed with caution since their resolution is quite poor and their underlying physical assumptions lead to a substantial underprediction of the sizes of present-day disks.

Our models allow a more detailed study of the sizes and cross-sections of high redshift disks than does that of Kauffmann (1996b). Figure 9 shows how the predicted abundance of absorbers at $z = 2.5$ rises as disks within lower and lower mass haloes are allowed to contribute. We parametrize the mass of the smallest contributing halo by $V_l$, the rotation velocity of its central disk measured at $3R_d$ and averaged over the $\lambda$-distribution of stable disks. This abundance refers to absorbers with $N_{\rm HI} > N_l$ and is calculated from

$$\begin{aligned} n(z) &= \frac{\pi}{2}(1+z)^3 \frac{dl}{dz} \int d\lambda p(\lambda) \int_{N_l}^{\infty} \frac{dN_{\rm HI}}{N_{\rm HI}^3} \int_{M_l}^{\infty} dM n_h(M,z) R_d^2(M,\lambda,z) \\ &\times N_0^2(M,\lambda,z)(1+2x_1)e^{-2x_1}\Theta(\epsilon_{\rm m} - \epsilon_{\rm m,crit}), \end{aligned} \tag{41}$$

where $l(z)$ is the proper distance at redshift $z$, $n_h(M,z)dM$ is the comoving number density of galactic haloes given by equation (A5), $N_0$ is the central column density of the disk, $N_l = 2 \times 10^{20}\,{\rm cm}^{-2}$ is the minimum HI column density for a DLS, and

$x_1 = -\ln[\min(1, N_{\rm HI}/N_0)]$. The step function, $\Theta(x) = 1$ for $x > 0$ and $\Theta(x) = 0$ for $x \leq 0$, ensures that only stable disks are used. For this plot we assume $m_d = j_d = 0.05$ and $\epsilon_{\rm m,crit} = 1$. We also assume that all baryons at the outer edge of the absorbing region are in the form of HI gas, and that the column density never drops below $N_l$ at smaller radii. This may be unrealistic at low redshift because star formation may substantially reduce the mass of HI gas. The horizontal dotted lines show a $\pm 2\sigma$ range for the observed DLS abundance at $z = 2.5$, taken from Storrie-Lombardi et al (1996). The lower limit on $V_l$ needed to reproduce the observations can be read off immediately. This limit varies quite strongly between cosmogonies. For $\tau$CDM, which has the smallest power on galactic scales, one has to include disks with rotation velocities smaller than $50\,{\rm km\,s^{-1}}$. This confirms the result found earlier for the MDM model which has a similar power spectrum (Mo & Miralda-Escudé 1994; Kauffmann & Charlot 1994; Ma & Bertschinger 1994; Klypin et al 1995). For the other three models, about one third of the observed systems can arise in disks with $V_c \gtrsim 200\,{\rm km\,s^{-1}}$, and two thirds or more in disks with $V_c \gtrsim 100\,{\rm km\,s^{-1}}$. It may not be difficult to accommodate disks with $V_c$ as large as suggested by Wolfe and collaborators, although these will be predicted to be much smaller at $z = 2.5$ than nearby disks with the same circular velocity.

It is interesting that the total cross-section of rotationally supported *stable* disks with $V_c \gtrsim 100\,{\rm km\,s^{-1}}$ can already explain the observations. Unless the formation of such disks is prevented, they should give rise to a large fraction of the observed DLS. Some absorbers may correspond to *unstable* disks, but the abundance of this population should be relatively small; such disks are compact and so have small cross-sections. Figure 10 shows the cross-section weighted distribution of the spin parameter for disks at $z = 2.5$. Comparing this with the unweighted $\lambda$-distribution (shown as the dot-dashed curve), we see that absorption comes primarily from disks with large $\lambda$. For $m_d = j_d = 0.05$, $\lambda_{\rm crit} \approx 0.05$, and less than 20% of DLS are produced by unstable systems (assuming, of course, that instability does not change the cross-section). The value of $n(z)$ for stable disks is maximised for $m_d \sim 0.05$, but varies little for $m_d$ $(= j_d)$ in the range from 0.025 to 0.07. The abundance is smaller both for larger and for smaller $m_d$, in the first case because the number of stable disks is small, and in the second because the amount of gas is small. This range is similar to the one we inferred in earlier sections from the properties of local disk galaxies. As shown by Haehnelt et al (1997) many DLS may be produced by gas which has not fully settled into centrifugal equilibrium. We are implicitly assuming that the cross-section for damped absorption does not vary strongly, at least on average, over this settling period.

It is also instructive to look at the predicted distribution of the impact parameter $b$, defined as the distance between the line-of-sight and the centre of a disk which produces a

DLS. This distribution can be written as

$$P(b)db \propto db \int d\lambda p(\lambda) \int_{M_l}^{\infty} dM n_h(M,z) F[N_0(M,\lambda,z)/N_l, b, R_d(M,\lambda,z)]\Theta(\epsilon_{\rm m}-1), \quad (42)$$

where $M_l$ is the lower limit on halo mass, and $F$ is the distribution of $b$ for a disk with scalelength $R_d$ and central surface density $N_0$ observed at a random inclination angle. The function $F$ can be obtained from simple Monte-Carlo simulations. The solid curves in Figure 11 show $P(b)$ at $z = 2.5$, with $M_l$ chosen to reproduce the observed abundance of DLS. For $\tau$CDM, this distribution is narrow and peaks at quite small values of $b$; DLS at large impact parameters are rare in this model. For the other three models, however, the upper quartile of the distribution is at $\sim 5\,h^{-1}$kpc, so systems with relatively large impact parameter do occur. Not surprisingly, they tend to be associated with high-$V_c$ disks, as can be seen from the dashed curves. At present, there are very few measurements of the impact parameter for a high redshift DLS. Djorgovski et al (1996) have identified a galaxy responsible for a DLS at $z = 3.15$, and for this case the impact parameter is about $13\,h^{-1}$kpc (for $q_0 = 0.1$). An observation by Lu et al (1997) suggests that this is indeed a rotating disk, with $V_c \sim 200\,{\rm km\,s^{-1}}$. As one can see from Figure 11, for this $V_c$, the observed impact parameter is not exceptionally large. One cannot draw any statistical conclusions from a single event, but if systems like this turn out to be common the $\tau$CDM model would be disfavored.

It is worth noting that this consistency with the observational results requires that $m_d$ be in the range 0.025 to 0.07, and that little angular momentum be transferred to the dark halo during disk formation. Significant angular momentum loss would produce smaller disks. Haloes with smaller $V_c$ would then have to be included in order to match the observed abundance. In this case, typical DLS would be predicted to have smaller $V_c$ and smaller $b$, but to have larger column densities. Substantial star formation would be required to reduce the column densities to the observed values, contradicting, perhaps, the low metal abundances measured in high redshift DLS.

The galaxies responsible for DLS are likely to be easier to identify at lower redshift. It is therefore interesting to give predictions for such systems. As an example, we show the impact parameter distribution for DLS at $z = 1$ in Figure 12. Results are shown only for SCDM and $\Lambda$CDM; those for CCDM and $\tau$CDM are similar. The redshift is chosen to be typical for the low-redshift DLS observed by, for example, Steidel et al (see Steidel 1995). In computing this distribution we have used only disks with $V_c = 100 - 300\,{\rm km\,s^{-1}}$. This choice is based on the fact that disks with smaller $V_c$ are difficult to identify, while those with larger $V_c$ are rare. An upper limit on $V_c$ has to be imposed in our calculation, because massive haloes are likely to host elliptical galaxies or galaxy clusters which contain only a small amount of HI gas. The median and the upper quartile of the distribution are at about

7 and $10\,h^{-1}$kpc, respectively (see the solid curves). Larger impact parameters are expected for samples biased towards galaxies with larger $V_c$ (see the dashed curves). As before, of course, these predictions assume that star formation has not substantially reduced the gas column near the damped absorption boundary. Some decrease in impact parameter may therefore be expected by $z = 1$. However, the absorption cross-section of an exponential disk depends only logarithmically on $m_d$, and so Figure 12 will not change much provided star formation is only moderately efficient in the outer galaxy. On the other hand, the HI mass in a DLS decreases in proportion to $m_d$, so that systems observed at lower redshift may have systematically lower column densities and so give rise to a smaller cosmic density parameter in HI. These trends are indeed observed (Wolfe 1995), and arise naturally in models which take star formation into account (Kauffmann & Charlot 1994; Kauffmann 1996b).

To see what kind of disks produce DLS at low redshifts, we can examine the cross-section weighted distribution of the spin parameter. This distribution depends only weakly on $z$, so that Figure 10 is still relevant. Notice again the strong bias towards the large $\lambda$ tail. As discussed in §3, the disks which form in haloes with large $\lambda$ have large size and low surface densities. We thus expect that galaxies selected as DLS will be biased towards low surface densities. As noted by McGaugh & de Blok (1996) and others, the star formation rates in such galaxies are low, giving rise to low surface brightnesses, and producing a relatively small reduction in their cross-section for damped absorption. The impact parameter distribution of Figure 12 may then apply. There are now some observations of galaxies responsible for low redshift DLS. Steidel et al (see Steidel 1995) find the typical impact parameter for such systems to be 5-15 $h^{-1}$kpc. There are also indications that these galaxies tend to be blue, with low surface brightness (Steidel 1995) and low chemical abundance (Pettini et al 1995). All these points seem to agree well with our expectations. Obviously, more such data will provide stringent constraints on disk formation models of the kind we propose here.

## 5. THE EFFECT OF A CENTRAL BULGE

So far we have considered galaxies to contain only disk and halo components. In reality, most spirals also contain a bulge. For a galaxy of Milky Way type or later, the bulge mass is less than 20 percent that of the disk, so its dynamical effects are small. For earlier-type spirals, however, the bulge makes up a larger fraction of the stellar mass, and its effects may be significant. In this section we use a simple model to assess how our results are affected by the presence of a central bulge. We assume bulges to be point-like, to have a mass which

is $m_b$ times that of the halo, and to have negligible angular momentum. Further, we assume either that the specific angular momentum of the disk is the same as that of its dark halo (so that $j_d = m_d$ as usually assumed above), or that the total specific angular momentum of the stellar components is equal to that of the halo (so that $j_d = m_d + m_b$). The second case may be appropriate if angular momentum transfer to the halo is negligible, if low angular momentum gas forms the bulge, and if high angular momentum gas settles into the disk.

Under these assumptions it is straightforward to extend the model of Section 2.2 to include the bulge. Equation (25) becomes

$$M_f(r) = M_d(r) + M(r_i)(1 - m_d - m_b) + M_b, \tag{43}$$

and $V^2_{c,DM}$ in equations (30) and (31) is replaced by $V^2_{c,DM}(r)+V^2_{c,b}(r)$, where $V^2_{c,b}(r) = GM_b/r$ is the contribution to the circular velocity from the bulge. With these changes, the procedure of Section 2.2 can be applied as before to obtain the disk scalelength, $R_d$, and the rotation curve, $V_c(R)$.

In Figure 13 we show the predicted rotation curves when disk and bulge masses are equal. Results are shown for the two cases mentioned above, namely $j_d = m_d$ and $j_d = m_d + m_b = 2m_d$. The same total halo mass and concentration are adopted as in the top left panel of Figure 2. The rotation curves now diverge at small radius because of our unrealistic assumption of a point-like bulge. In the case where $j_d = 2m_d$ the disk is substantially more extended, and the value of $V_c$ at given radius is slightly lower, than in the case where $j_d = m_d$.

To see the effect of the central bulge more clearly, we compare values of $R_d$ and $V_c(3R_d)$ for the two cases, $M_b = M_d$ and $M_b = 0$. Figure 14 shows how the relative values vary with $m_d + m_b$. This figure assumes $\lambda = 0.05$ and $c = 10$, but in fact the ratios are quite insensitive to $\lambda$ and $c$. As one can see, for $j_d = m_d$ the values of $R_d$ and $V_c$ do not change much even when half of the accreted gas is put into the central bulge. On the other hand, for $j_d = 2m_d$, the disk scalelength increases by a factor of two, and the rotation velocity drops significantly below that for $M_b = 0$. This case produces similar results to those for $\lambda = 0.1$ and $M_b = 0$.

The results in Figure 14 have some interesting implications. If disks have the same specific angular momentum as their dark haloes, and if the luminosity of a galaxy is proportional to its total stellar mass, then the zero-point of the TF relation is almost independent of the mass of the bulge. Even in the extreme case where $M_d = M_b$ and disks have twice the specific angular momentum of their haloes, the disk rotation velocity for given $M_d + M_b$ is only reduced by about 20 percent provided $m_d + m_b \lesssim 0.1$. If disk and bulge had the same mass-to-light ratio, this would change the zero-point of the TF relation

by about $-0.8$ mag, but since the stellar mass-to-light ratio of bulges is undoubtedly higher than that of disks, the actual change would be smaller. In practice, most of the galaxies used in applications of the TF relation have bulge-to-disk ratios much smaller than one, so we expect the effects of the bulges to produce rather little scatter in the TF relation.

## 6. DISCUSSION

In this paper, we have formulated a simple model for the formation of disk galaxies. Although many of the observed properties of spirals and damped Ly$\alpha$ absorbers seem relatively easy to explain, it is important to keep in mind our underlying assumptions. These leave open a number of difficult physical questions. We have assumed that all galaxy haloes have the universal density profile proposed by NFW. This appears relatively safe since the original NFW claims have been confirmed by a number of independent N-body simulations (e.g. Tormen et al 1996; Cole & Lacey 1996; Huss et al 1997). More significantly we assume that all disks have masses and angular momenta which are fixed fractions of those of their haloes. Successful models require $M_d/M \gtrsim 0.05$ and $J_d/J \approx M_d/M$. These relations are not produced in a natural way by existing simulations of hierarchical galaxy formation. While it is common to find all the gas associated with galactic haloes within condensed central objects (so that $M_d \propto M$), the gas usually loses most of its angular momentum to the dark matter during galaxy assembly. This results in $J_d/J \ll M_d/M$ and produces disks which are too small (Navarro & Benz 1991; Navarro & White 1994; Navarro & Steinmetz 1997). The resolution of this problem may be related to the well-known need to introduce strong feedback in order to get a viable hierarchical model for galaxy formation (e.g. White & Rees 1978; White & Frenk 1991; Kauffmann et al 1993). Such feedback is not included in the simulations, but is required in hierarchical models to suppress early star formation in small objects, thus ensuring that gas remains at late times to form large galaxies and the observed intergalactic medium. Disks may then form from gas which remains diffuse and so loses little angular momentum during protogalactic collapse. Unfortunately, while such effects may solve the angular momentum problem, they call into question the proportionality between disk mass and halo mass. The disk/halo mass ratios required by our models are, in any case, much less than the observed baryon mass fractions in rich galaxy clusters, so substantial inefficiency in assembling the galaxies is necessary in any consistent model.

There are several interesting theoretical issues that are not addressed in this paper. As is well known, disk galaxies, especially LSB galaxies, have lower correlation amplitudes than ellipticals (see e.g. Davis & Geller 1976; Jing, Mo & Börner 1993; Mo, McGaugh

& Bothun 1994). Since hierarchical clustering predicts little correlation between the spin parameter of a halo and its large-scale environment, this observed clustering difference cannot be considered a consequence of disk galaxies being associated with haloes with large $\lambda$. However, as discussed above, disk galaxies, especially LSBs, form late in our model. On the other hand, elliptical galaxies, and in particular cluster ellipticals, form at relatively high redshifts in hierarchical models (Kauffmann 1996a). Since for given mass, haloes at low redshift are less correlated than those at high redshift (Mo & White 1996), the morphology dependence of clustering can arise as a consequence of the morphology dependence of formation time. This effect is seen quite clearly in the detailed semianalytic galaxy formation models of Kauffmann et al (1993) and Kauffmann, Nusser & Steinmetz (1997). Local environmental effects may also lead to morphological segregation; for example, extended disks may be destroyed in a high density environment by tidal effects and gas stripping (Moore et al 1996). Detailed modelling is clearly needed for any quantitative comparison with observation.

In this paper we have considered the formation of disk galaxies only. It is interesting to examine how other populations might fit into such a scenario. Earlier semianalytic modelling has shown that many of the global properties of giant ellipticals can be understood if they formed by mergers between disk systems which themselves formed at early times in overdense "protocluster" regions. As we have seen, high redshift disks should be substantially denser and more compact than present-day disks of similar mass. This may go a long way towards explaining the high densities of observed ellipticals. Some bulges and ellipticals may also form in dark haloes with low spin where any disk would be too dense to be stable. Such "spheroidal" systems may have systematically different properties from those which formed by mergers. We intend to return to a number of these issues in future papers.

We are grateful to S. Courteau for providing the data plotted in Figure 4. We thank Luiz da Costa for helpful discussions. This project is partly supported by the "Sonderforschungsbereich 375-95 für Astro-Teilchenphysik" der Deutschen Forschungsgemeinschaft.

## REFERENCES

Bardeen J., Bond J.R., Kaiser N., Szalay A.S., 1986, ApJ, 304, 15

Barnes J., White S.D.M. 1984, MNRAS, 211, 753

Baugh C.M., Cole S., Frenk C.S., Lacey C.G. 1997, preprint (astro-ph/9703111)

Bertschinger, E. 1985, ApJS, 58, 39

Bessel M.S., 1979, PASP, 91, 589

Binney J., Tremaine S., 1987, Galactic Dynamics. Princeton Univ. Press, Princeton, NJ

Bothun G., Impey C., McGaugh S., 1997, preprint (astro-ph/9702156)

Bottema, R. 1997, preprint (astro-ph/9706230)

Broeils A.H., Courteau S., 1996, preprint (astro-ph/9610264)

Carroll S.M., Press W.H., Turner E.L., 1992, ARAA, 30, 499

Casertano S. Van Gorkom J., 1991, AJ, 101, 1231

Christodoulou D.M., Shlosman I., Tohline J.E., 1995, ApJ, 443, 551

Cole S., Aragon-Salamanca A., Frenk C.S., Navarro J.F., Zepf S. E., 1994, MNRAS, 271, 781

Cole S., Lacey C., 1996, preprint (astro-ph/9510147 v3)

Courteau S., 1996, ApJS, 103, 363

Courteau S., 1997, ApJS, 1in press

Dalcanton J.J., Spergel D.N., Summers, F.J., 1997, ApJ, 482, 659 (DSS)

Davis M., Geller M., 1976, ApJ, 208, 13

Djorgovski S.G., Pahre M.A., Bechtold J., Elston R., 1996, Nature, 382, 234

Efstathiou G., Bond J.R., White S.D.M., 1992, MNRAS, 258, 1P

Efstathiou G., Lake, G., Negroponte, J., 1982, MNRAS, 199, 1069

Eisenstein, D.J., Loeb, A., 1996, ApJ, 459, 432

Fall S.M., Efstathiou G., 1980, MNRAS, 193, 189

Gardner J.P., Katz N., Weinberg D.H., Hernquist L., 1997, preprint (astro-ph/9705118)

Giovanelli R., Haynes M.P., da Costa L.N., Freudling W., Salzer J.J., Wegner G., 1997, preprint (astro-ph/9612072)

Gunn J., Gott R., 1972, ApJ, 176, 1

Haehnelt M. G., Steinmetz M., Rauch, M., 1997, preprint (astro-ph/9706201)

Huss A., Jain B., Steinmetz M., 1997, preprint (astro-ph/9703014)

Jedamzik, K., Prochaska, J.X. 1997, preprint (astro-ph/9706290)

Jing Y.P., Mo H.J. & Börner G., 1991, A&A, 252, 449.

Katz N., Gunn J., 1991, ApJ, 377, 365

Kauffmann G., Charlot S., 1994, ApJ, 430, L97

Kauffmann G., White S.D.M., Guiderdoni B., 1994, MNRAS, 267, 981

Kauffmann G. 1996a, MNRAS, 281, 487

Kauffmann G. 1996b, MNRAS, 281, 475

Kauffmann G., Nusser A., Steinmetz M., 1997, MNRAS, 286, 795

Klypin A., Borgani S., Holtzman J., Primack. J., 1995, ApJ, 444, 1

Lacey C., Cole S., 1993, MNRAS, 262, 627

Lacey C., Cole S., 1995, preprint (astro-ph/9510147)

Lanzetta K.M., Wolfe A. M., Turnshek D. A., 1995, ApJ, 440, 435L

Lu L., Sargent W.L.W., Barlow T.A., 1997, preprint (astro-ph/9701116)

Ma C.P., Bertschinger E., 1994, ApJ, 434, L5

McGaugh S.S., 1994, Nature, 367, 538

McGaugh S.S., de Blok W.J.G., 1996, preprint (astro-ph/9612070)

Mo H.J., Jing Y.P., White S.D.M., 1996, MNRAS, 282, 1096

Mo H.J., McGaugh S.S., Bothun G.D., 1994, MNRAS, 267, 129

Mo H.J., Miralda-Escudé J., 1994, ApJ, 430, L25

Mo H.J., White S.D.M., 1996, MNRAS, 282, 347

Moore B., Katz N., Lake G., Dressler A., Oemler, A. Jr., 1996, Nature, 379, 613

Navarro J.F., Benz W. 1991, ApJ, 380, 320

Navarro J.F., White S.D.M., 1994, MNRAS, 267, 401

Navarro J.F., Frenk C. S., White S.D.M., 1995, MNRAS, 275, 720

Navarro J.F., Frenk, C. S., White, S.D.M., 1996, ApJ, 462, 563

Navarro J.F., Frenk, C. S., White, S.D.M., 1997, in press (preprint, astro-ph/9611107) (NFW)

Navarro J.F., Steinmetz M., 1997, 478, 13

Pettini M., King D.L., Smith L.J., Hunstead R.W., 1995 in QSO Absorption Lines, ed. G. Meylan, Springer: Berlin, p.71

Press W.H., Schechter P., 1974, ApJ, 187, 425 (PS)

Prochaska J.X., Wolfe A.M., 1997, ApJ, submitted

Percic, M., Salucci, P., 1991, ApJ, 285, 307

Shanks T., 1997, preprint (astro-ph/9702148)

Sprayberry D., Bernstein G.M., Impey C.D., Bothun G.D., 1995, ApJ, 438, 72

Steidel C.C., 1995, in QSO Absorption Lines, ed. G. Meylan, Springer: Berlin, p.137

Steinmetz M., Bartelmann M., 1995, MNRAS, 272, 570

Steinmetz M., Müller E., 1995, MNRAS, 276, 549

Storrie L.J., McMahon R.G., Irwin M.J., 1996, MNRAS, 283, L79

Strauss, M., Willick, J.A., 1995, Phys. Reports, 261, 271

Toomre A., 1964, ApJ, 139, 1217

Tormen G., Bouchet F.R., White S.D.M., 1997, MNRAS, 286, 865

Turner, M.S. 1996, preprint (astro-ph/9610158)

Walker T. P., Steigman, G., Schramm, D. N., Olive, K. A., Kang, H.-S. 1991, ApJ 376, 51

Warren M.S., Quinn P.J., Salmon J.K., Zurek W.H., 1992, ApJ, 399, 405

White M., Scott D., 1996, Comments on Astrophysics, 8, No. 5

White S.D.M., 1995, Les Houches

White S.D.M., Efstathiou G., Frenk C., 1993, MNRAS, 262, 1023

White S.D.M., Frenk C.S., 1991, ApJ, 379, 52

White S.D.M., Rees M.J., 1978, MNRAS, 183, 341

Williams R.E., et al, 1996, AJ, 112, 1335

Willick J.A., Courteau S., Faber S.M., Burstein D., Dekel A., Kolatt T., 1996, ApJ, 457, 460

Willick J.A., Courteau S., Faber S.M., Burstein D., Dekel A., 1995, ApJ, 446, 12

Wolfe A., Turnshek, D.A., Smith, H.E., Cohen, R. D., 1986, ApJS, 61, 249

Wolfe A., 1995, in QSO Absorption Lines, ed. G. Meylan, Springer: Berlin, p.13

Zwaan M.A., van der Hulst J.M., de Blok W.J.G., McGaugh S.S., 1995, MNRAS, 273, L35

## A. Cosmogonies

We assume that the universe is dominated by cold dark matter (CDM). The initial power spectrum is

$$P(k) \propto kT^2(k), \tag{A1}$$

with

$$T(k) = \frac{\ln(1+2.34q)}{2.34q}\left[1+3.89q+(16.1q)^2+(5.46q)^3+(6.71q)^4\right]^{-1/4} \tag{A2}$$

and

$$q \equiv \frac{k}{\Gamma h\,\mathrm{Mpc}^{-1}} \tag{A3}$$

(see Bardeen et al 1986). Following Efstathiou et al (1992), we have introduced a shape parameter, $\Gamma$, for the power spectrum. The RMS mass fluctuation in top-hat windows with radius $r_0$, $\sigma(r_0)$, is defined by

$$\sigma^2(r_0) = \frac{1}{2\pi^2}\int_0^\infty \frac{dk}{k}k^3P(k)W^2(kr_0), \tag{A4}$$

where $W(x)$ is the Fourier transform of the top-hat window function. The power spectrum, $P(k)$, is normalized by specifying $\sigma_8 \equiv \sigma(8\,h^{-1}\mathrm{Mpc})$.

We use the Press-Schechter formalism (Press & Schechter 1974) to calculate the mass function of dark haloes. In this formalism, the comoving number density of dark haloes, with mass in the range $M \to M+dM$, at redshift $z$ is

$$n_h(M,z)dM = -\left(\frac{2}{\pi}\right)^{1/2}\frac{\overline{\rho}_0}{M}\frac{\delta_z}{\sigma(r_0)}\frac{d\ln\sigma(r_0)}{d\ln M}\exp\left[-\frac{\delta_z^2}{2\sigma^2(r_0)}\right]\frac{dM}{M}, \tag{A5}$$

where $\overline{\rho}_0$ is the mean matter density of the universe at present time; $M$ is the mass of the halo, related to the initial comoving radius $r_0$ of the region from which the halo formed (measured in current units) by $M = \frac{4\pi}{3}\overline{\rho}_0 r_0^3$, $\delta_z$ is the threshold linear overdensity for collapse at redshift $z$. According to the spherical collapse model,

$$\delta_z = (1+z)\delta_c\frac{g(a_0)}{g(a)}, \tag{A6}$$

where $\delta_c \approx 1.68$ (see NFW); $g(a)$ is the linear growth factor at the expansion factor $a$ corresponding to the redshift $z$ ($a_0$, the present value of $a$, is taken to be 1):

$$g(a) = \frac{5}{2}\Omega \left[\Omega^{4/7} - \Omega_\Lambda + (1 + \Omega/2)(1 + \Omega_\Lambda/70)\right]^{-1} \tag{A7}$$

(see Carroll, Press & Turner 1992), with

$$\Omega \equiv \Omega(a) = \frac{\Omega_0}{a + \Omega_0(1-a) + \Omega_{\Lambda,0}(a^3 - a)}, \tag{A8}$$

$$\Omega_\Lambda \equiv \Omega_\Lambda(a) = \frac{a^3\Omega_{\Lambda,0}}{a + \Omega_0(1-a) + \Omega_{\Lambda,0}(a^3 - a)}. \tag{A9}$$

To put the NFW density profile in a cosmological context, we need to calculate the concentration factor $c$ defined in equation (20). For this density profile, $c$ is related to the characteristic overdensity, $\delta_0$, by equation (21). The appropriate value of $c$ depends on halo formation history and on cosmology. NFW proposed a simple model for $c$ based on halo formation time. The formation redshift $z_f$ of a halo identified at $z = 0$ with mass $M$ is defined as the redshift by which half of its mass is in progenitors with mass exceeding $fM$, where $f < 1$ is a constant. According to the formula given by Lacey & Cole (1993) based on the Press-Schechter formalism, the halo formation time is then defined implicitly by

$$\mathrm{erfc}\left[\frac{(\delta_{z_f} - \delta_c)}{\sqrt{2[\sigma^2(fM) - \sigma^2(M)]}}\right] = \frac{1}{2}. \tag{A10}$$

NFW found that the characteristic overdensity of a halo at $z = 0$ is related to its formation redshift $z_f$ by

$$\delta_0(M, f) = C(f)\Omega_0 \left[1 + z_f(M, f)\right]^3, \tag{A11}$$

where the normalization $C(f)$ depends on $f$. We will take $f = 0.01$ as suggested by the N-body results of NFW. In this case $C(f) \approx 3 \times 10^3$. Thus, for a halo of given mass at $z = 0$, one can obtain the concentration factor $c$ from equations (A6)-(A11). In practice, we first solve $z_f$ from equation (A10) and insert the value of $z_f$ into equation (A11) to get $\delta_0$, we then use this value of $\delta_0$ in equation (21) to solve for $c$. The distribution of $c$ is not well known. In the simulations of NFW, the scatter in $c$ is $\Delta c/c \approx 0.25$.

Equations (A10)-(A11) can be easily extended to calculate concentrations for haloes identified at $z > 0$. In this case, we just replace $\delta_c$ in equation (A10) by $\delta_z$, and $\Omega_0$ in equation (A11) by $\Omega(a)/(1+z)^3$, where $a$ is the scale factor at $z$.

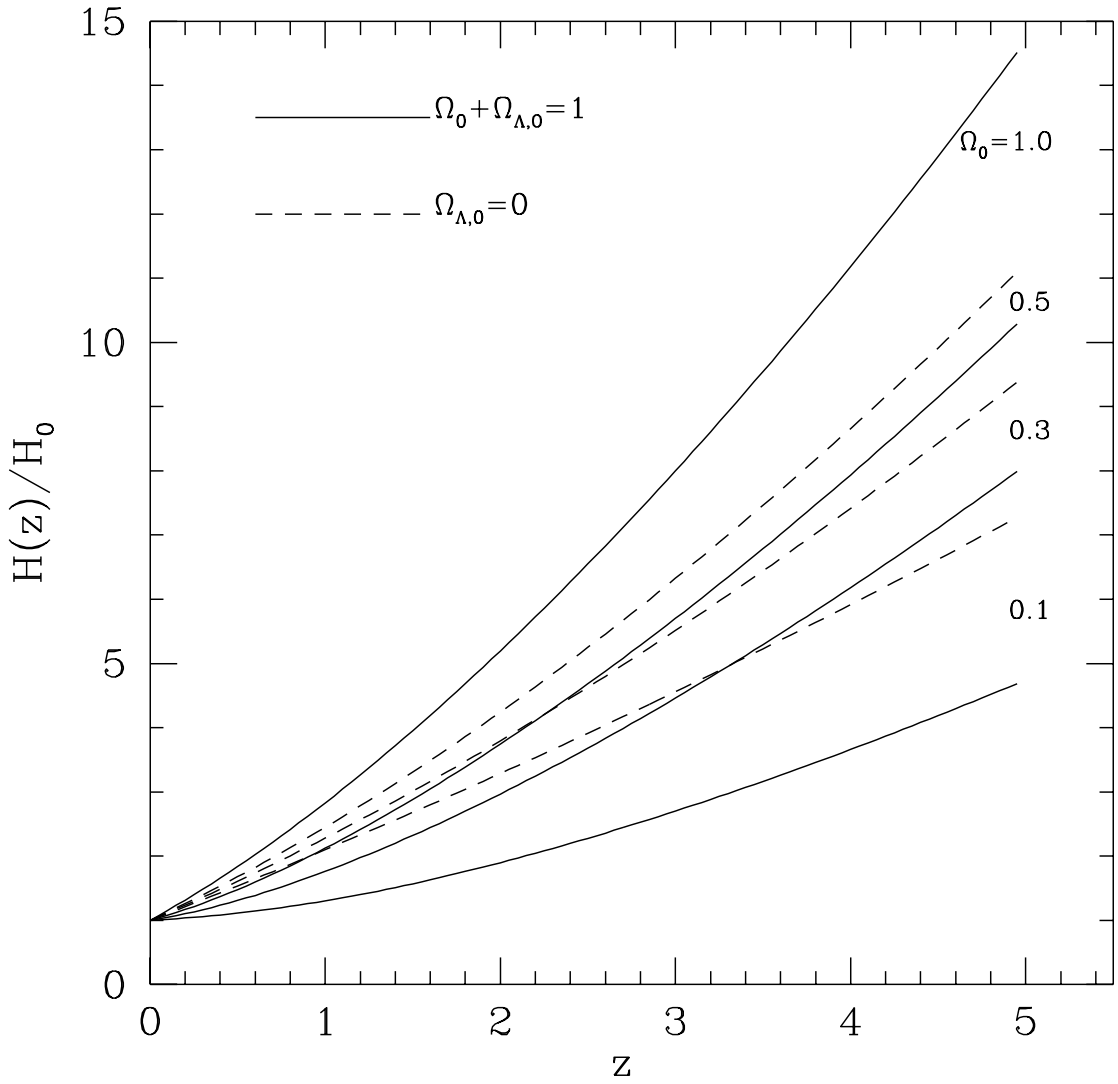


Fig. 1.— The Hubble constant (in units of its present value) as a function of redshift for flat ($\Omega_0 + \Omega_{\Lambda,0} = 1$) and open models with various $\Omega_0$.

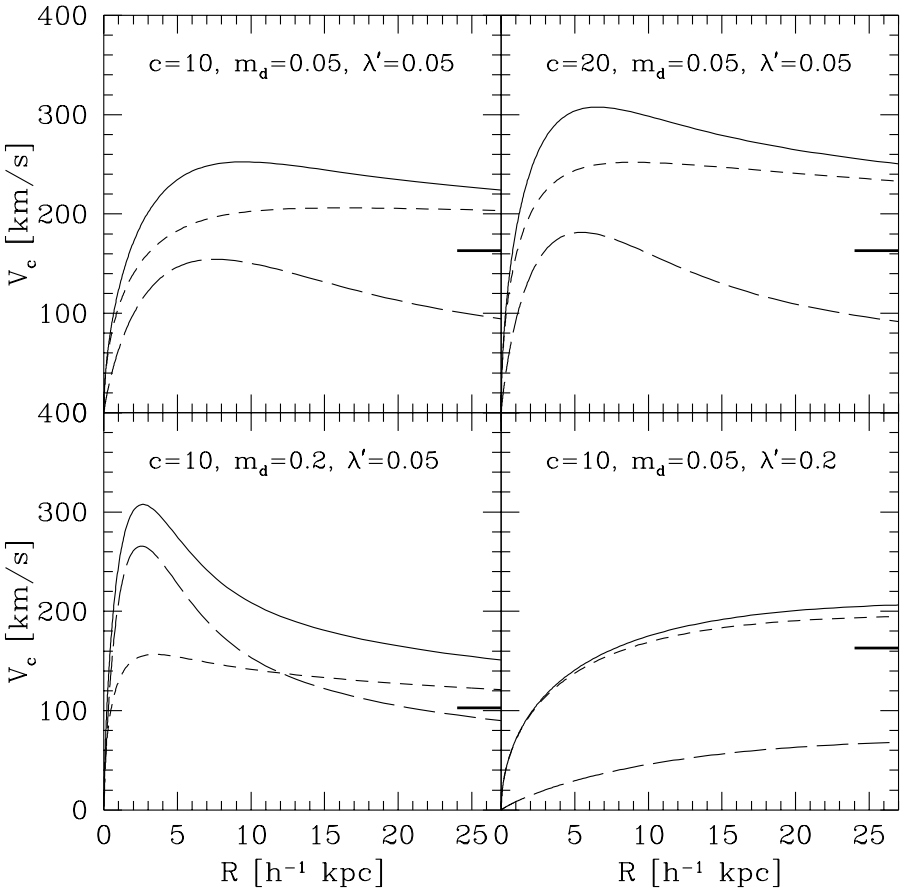


Fig. 2.— Rotation curves for disk galaxies formed in haloes with an initial density distribution described by the NFW profile. The shape of the rotation curves depends only on the concentration parameter, $c$, the fraction of mass in the disk, $m_d$, and the spin parameter, $\lambda' \equiv (j_d/m_d)\lambda$. The total mass of a halo determines both the disk scalelength and the amplitude of the rotation curve. Four panels are shown for different sets of $c$, $m_d$ and $\lambda'$. The disk mass is assumed to be $M_d = 5 \times 10^{10} h^{-1} M_\odot$. The rotation velocities induced by the disk and the dark matter are shown using long-dashed and short-dashed lines, respectively, while the total rotation velocity is shown by a solid line. The rotation velocity induced by the disk reaches a peak at about two disk scalelengths. The rotation velocity at $r_{200}$ is indicated by thick horizontal bars and is identical to the rotation velocity at all radii for a singular isothermal sphere with the same mass. The upper left panel should be viewed as the reference panel. Only one parameter is varied between this panel and any other. Notice how the prominence and amplitude of the peak in the rotation curve change between panels.

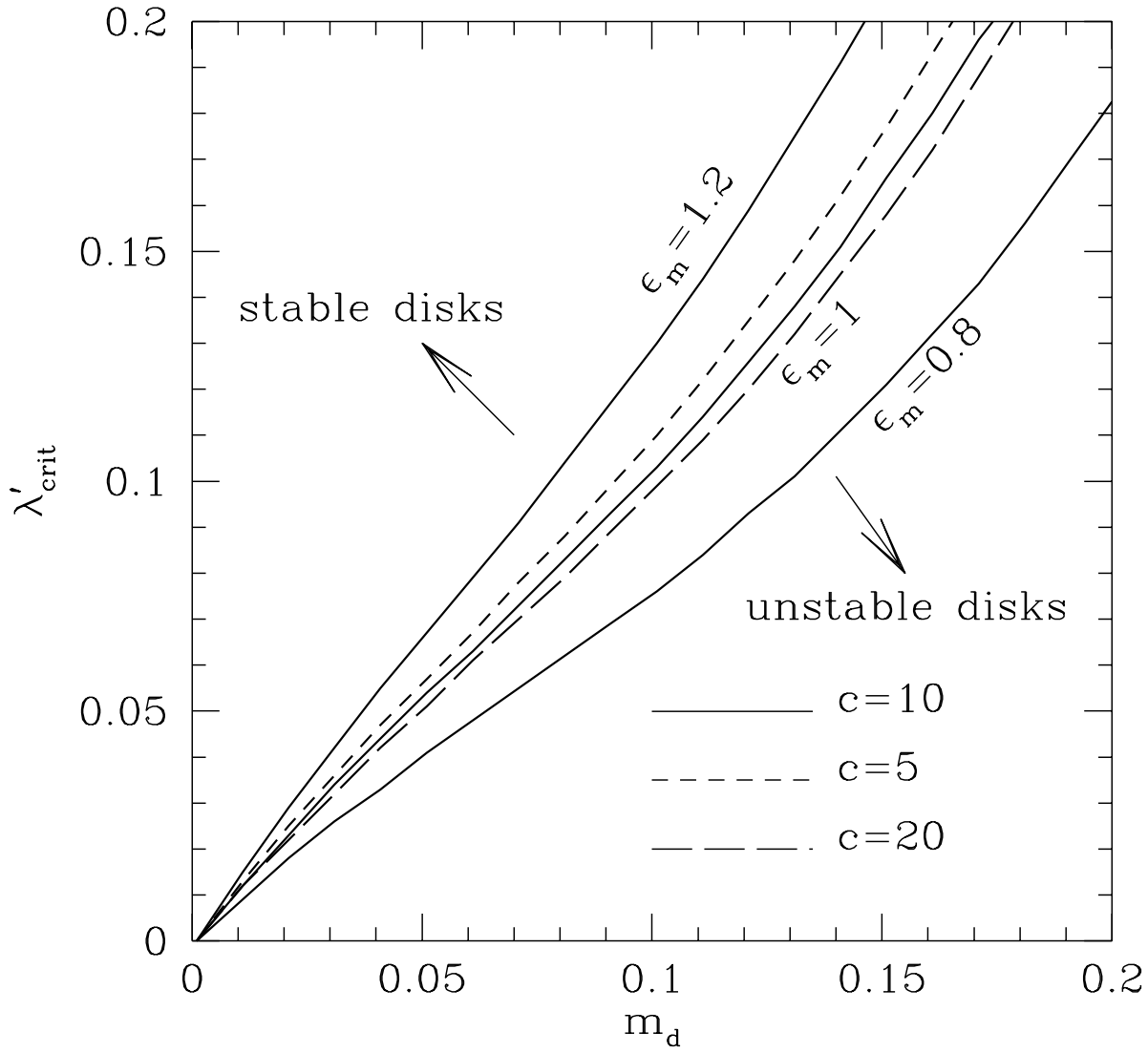


Fig. 3.— Critical values of $\lambda'$ ($\equiv \lambda j_d/m_d$) for disk instability as a function of $m_d$. Results are shown for three choices of $\epsilon_{\rm m}$. For a given $m_d$, disks are stable if $\lambda' > \lambda'_{\rm crit}$. The dependence on halo concentration, $c$, is weak, and is shown only for $\epsilon_{\rm m} = 1$.

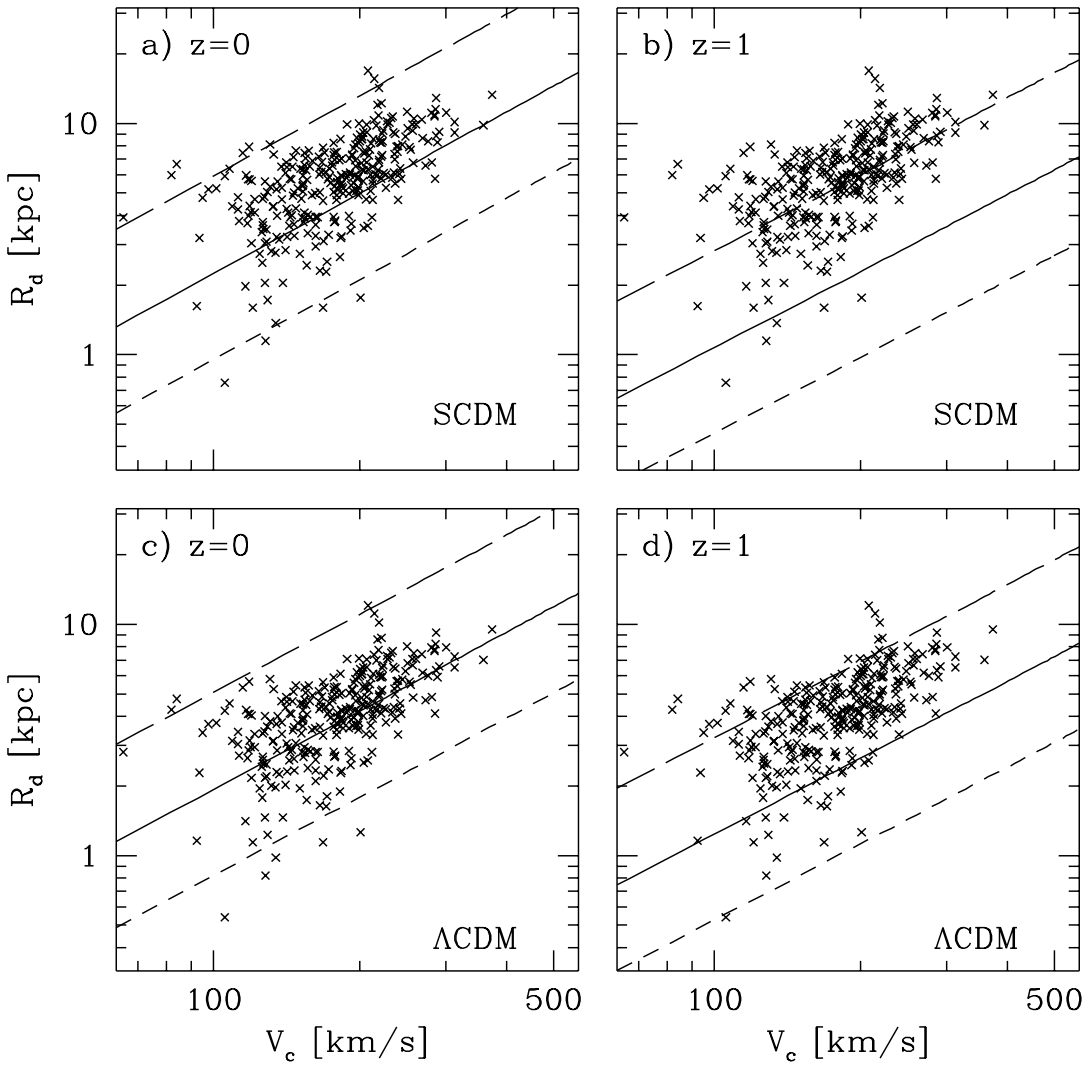


Fig. 4.— Model predictions for $R_d$ as a function of $V_c$ for stable disks assembled at $z = 0$ and at $z = 1$ in the SCDM and ΛCDM models. The solid lines give the relations for critical disks when $m_d = 0.05$, while short-dashed lines give the corresponding relations for $m_d = 0.025$. Stable disks must lie above the line for the relevant value of $m_d$. The long-dashed lines correspond to $m_d = j_d$ and $\lambda = 0.1$; at most 10% of disks should lie above these lines. The data points are the observational results of Courteau (1996; 1997) for a sample of nearby normal spirals.

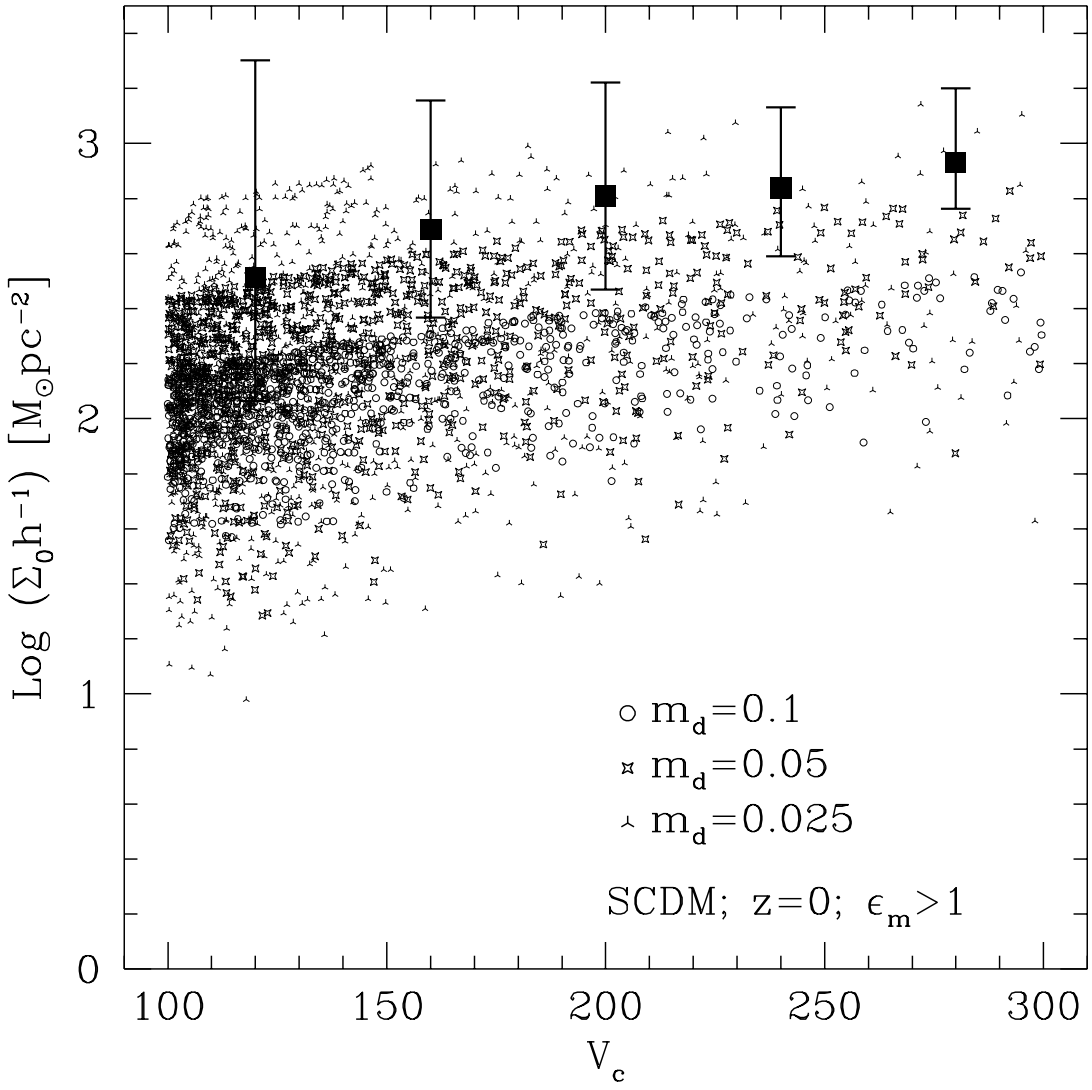


Fig. 5.— The distribution of central surface density for disks at $z = 0$ in the SCDM model. Results are shown assuming $m_d = j_d$ and for $m_d = 0.025$, 0.05 and 0.1. Only stable disks with $\epsilon_{\rm m} > 1$ are plotted. The squares with error bars refer to the observational data from Figure 4. The circular velocities have been converted to a luminosity using the Tully-Fisher relation of Giovanelli et al (1997), and this in turn has been converted into a mass using $\Upsilon_I = 1.7h$ (Bottema 1997). The square is plotted at the median value in each bin and the ends of the error bars mark the upper and lower 10% points of the distributions.

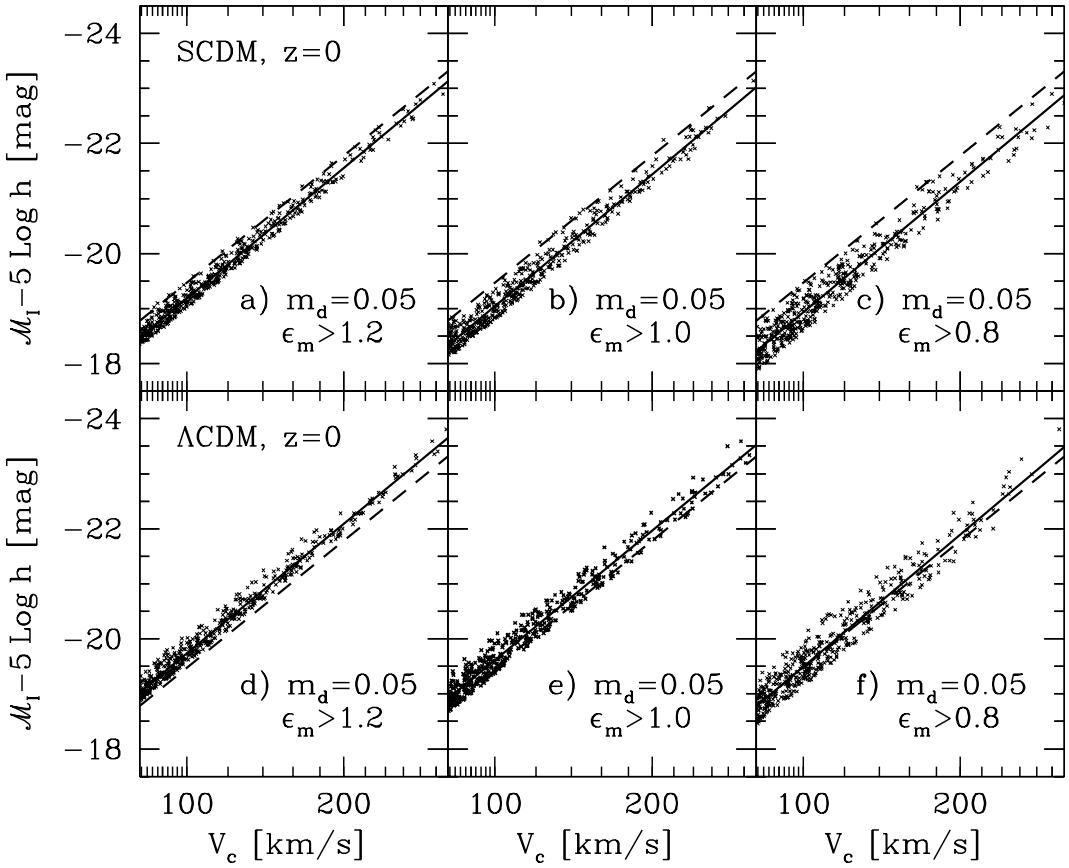


Fig. 6.— Tully-Fisher (TF) relations for stable disks at $z = 0$ in the SCDM and ΛCDM cosmogonies. Monte Carlo samples of the predicted luminosity-rotation velocity distribution are shown for three choices of $\epsilon_{\rm m}$. We have converted stellar mass (in the model) into I-band luminosity using $\Upsilon = 1.7h$ (Bottema 1997). The solid lines give the linear regressions of absolute magnitude against $\log V_c$. The dashed lines show the observed TF relation as given by Giovanelli et al (1997)

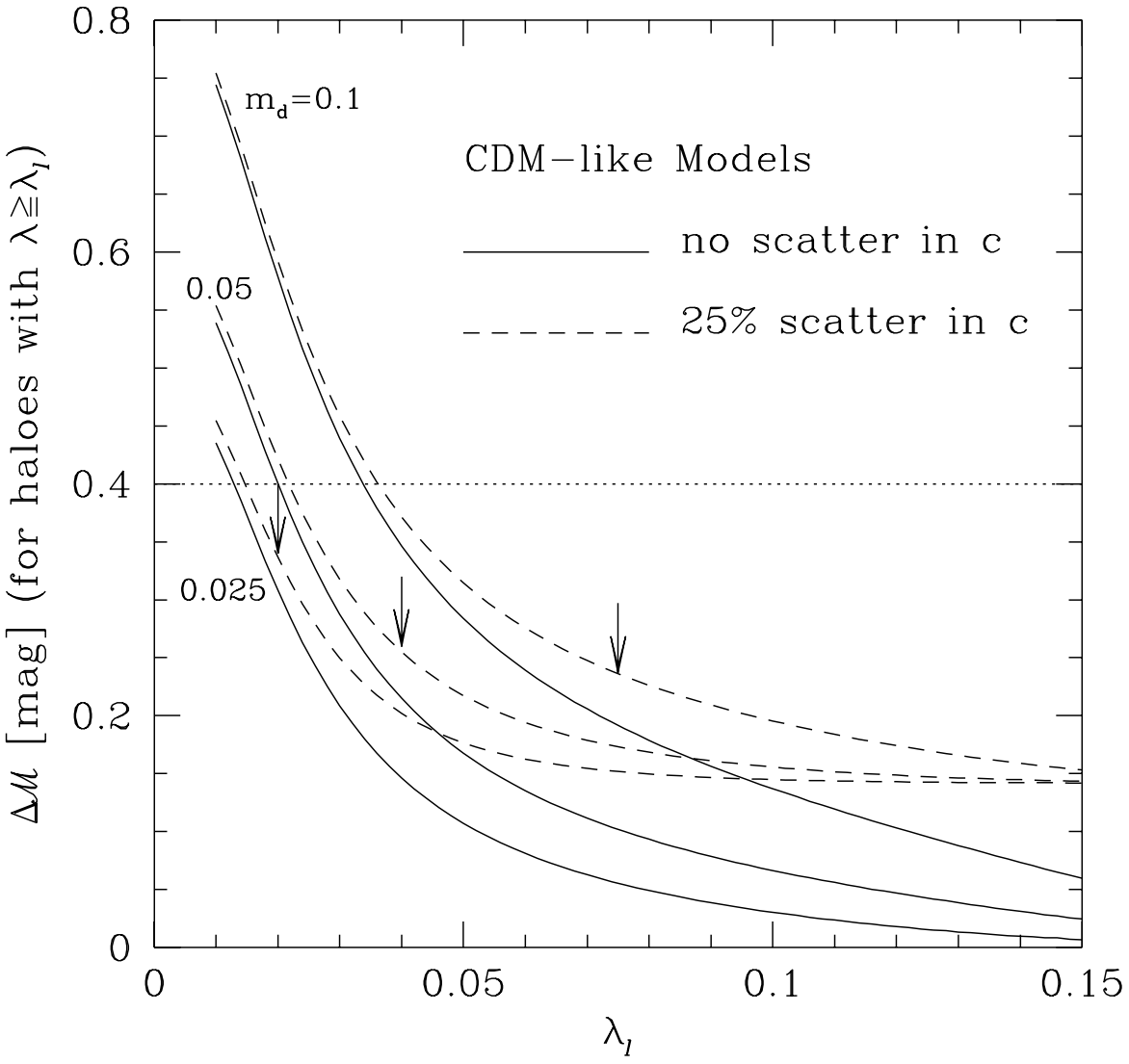


Fig. 7.— The scatter about the mean TF relation as a function of $\lambda_l$, the lower limit on $\lambda$ for the haloes included in the relation. The solid curves show results which ignore the scatter caused by variations of the halo concentration, $c$, while the dashed curves show assume an *rms* scatter of 25% in $c$. Three curves are shown for three different disk mass fractions, $m_d = 0.1, 0.05$ and $0.025$ (from top to bottom). The horizontal line shows the observed scatter for normal disk galaxies, as given by Willick et al (1996). The arrows mark the critical values of $\lambda$; disks are stable only for larger $\lambda$ values.

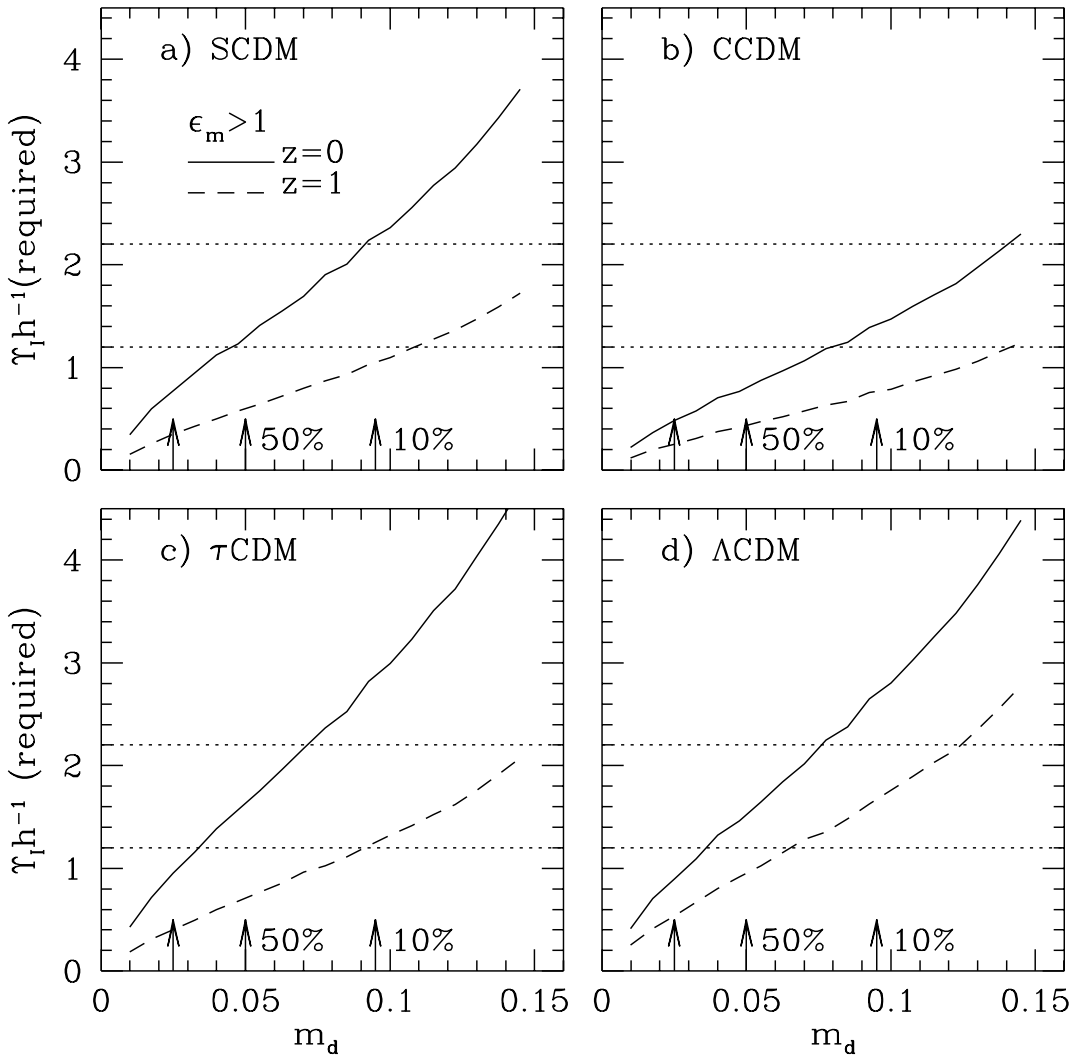


Fig. 8.— The mass-to-light ratio required to reproduce the observed zero-point of the TF relation as given by Giovanelli et al (1997). Stable disks with $\epsilon_{\rm m} > 1$ are used. Results are shown for two assembly redshifts, $z = 0$ (solid lines) and $z = 1$ (dashed lines). The horizontal lines bracket the values of $\Upsilon_I$ allowed by dynamical studies of disks (Bottema 1997). The arrows indicate the values of $m_d$ at which 90%, 50% and 10% of haloes can host stable disks.

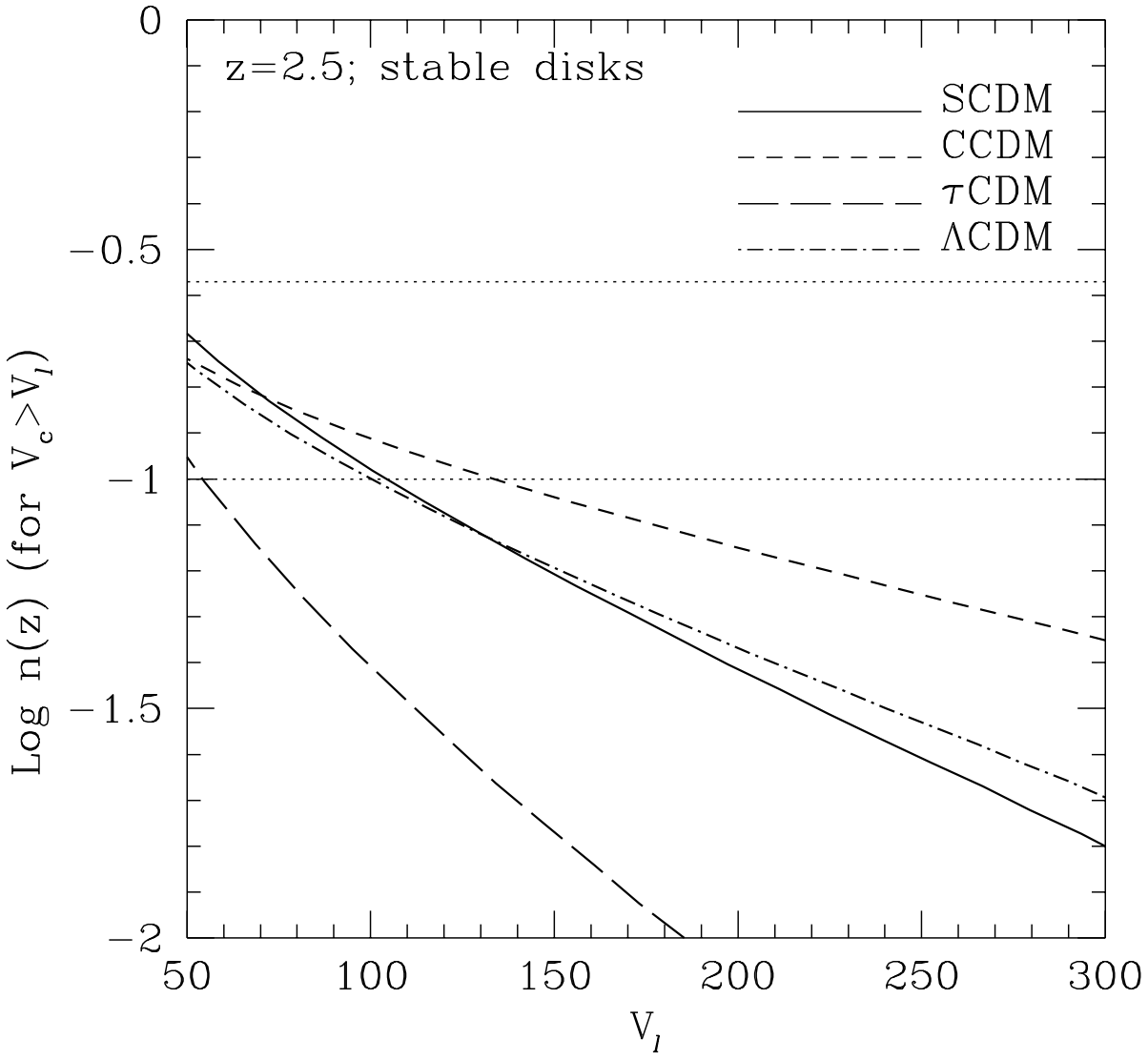


Fig. 9.— Logarithm of the predicted abundance of damped Ly$\alpha$ systems at $z = 2.5$ as a function of $V_l$, the rotation velocity of the least massive disks allowed to contribute. Only stable disks are assumed to give rise to damped Ly$\alpha$ systems (i.e. disks with $\epsilon_{\rm m} > 1$). The horizontal lines show the $\pm 2\sigma$ range of the observed abundance as given by Storrie-Lombardi et al (1996).

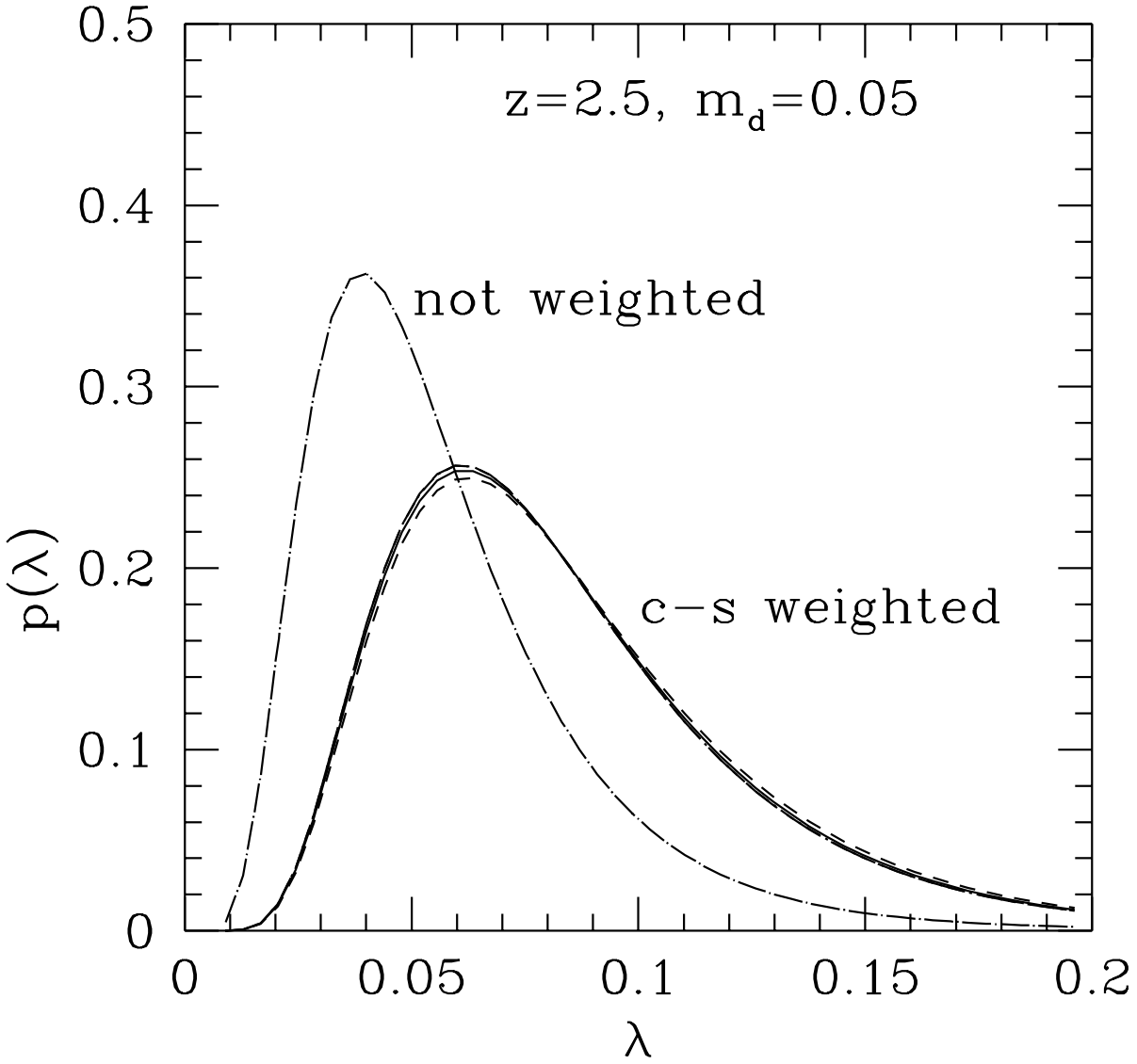


Fig. 10.— The cross-section (c-s) weighted distribution of halo spin at $z = 2.5$. Notice that this distribution depends only weakly on cosmogony; the curves corresponding to our four cosmogonies can barely be distinguished. The unweighted $\lambda$-distribution, as given by equation (15), is shown as the dot-dashed curve.

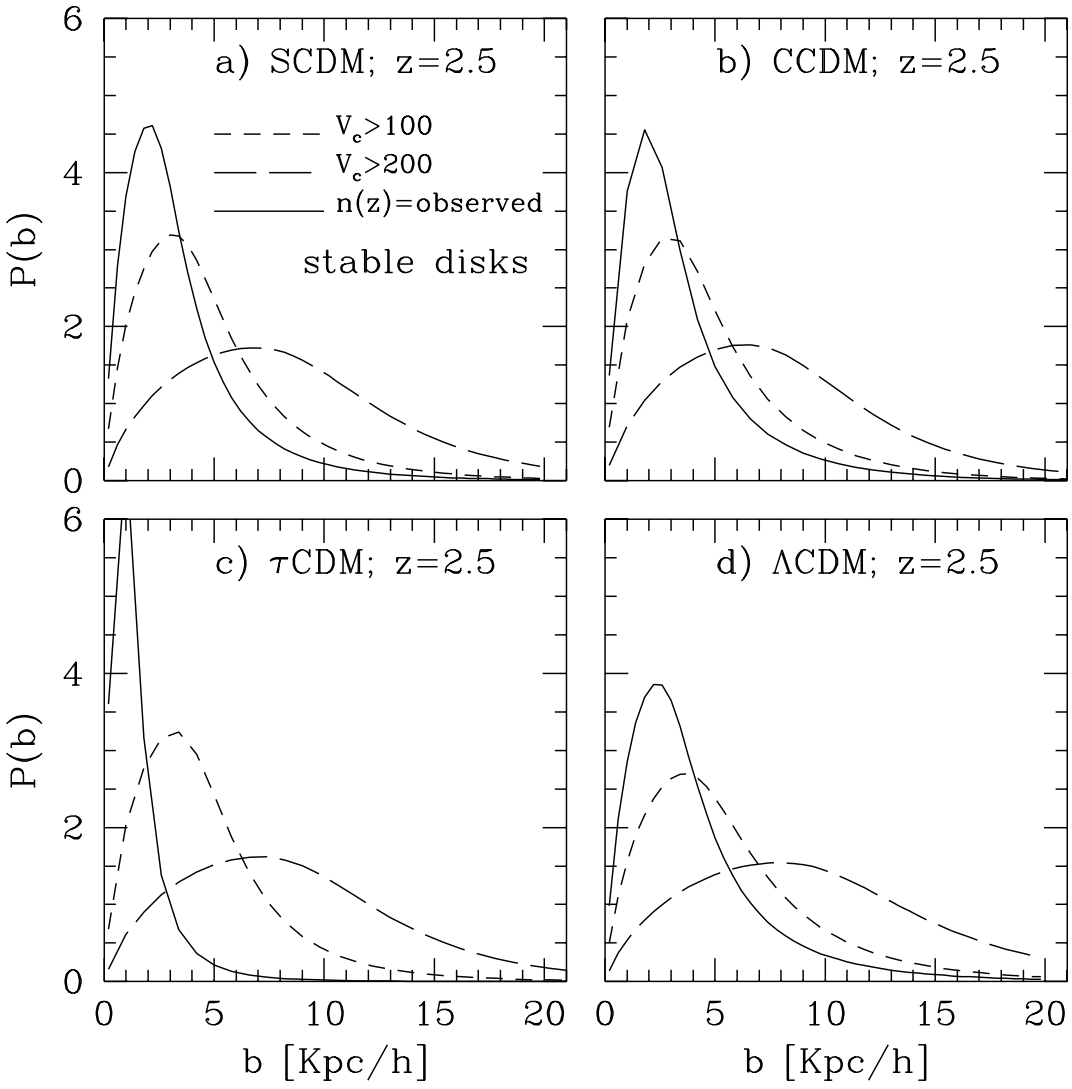


Fig. 11.— The distribution of impact parameter for damped systems in stable disks at $z = 2.5$. The solid curves show the results when the mass of the smallest contributing disks is chosen so that the predicted abundance of absorbers is equal to the observed value. The dashed curves show the results when only disks with large $V_c$ are selected.

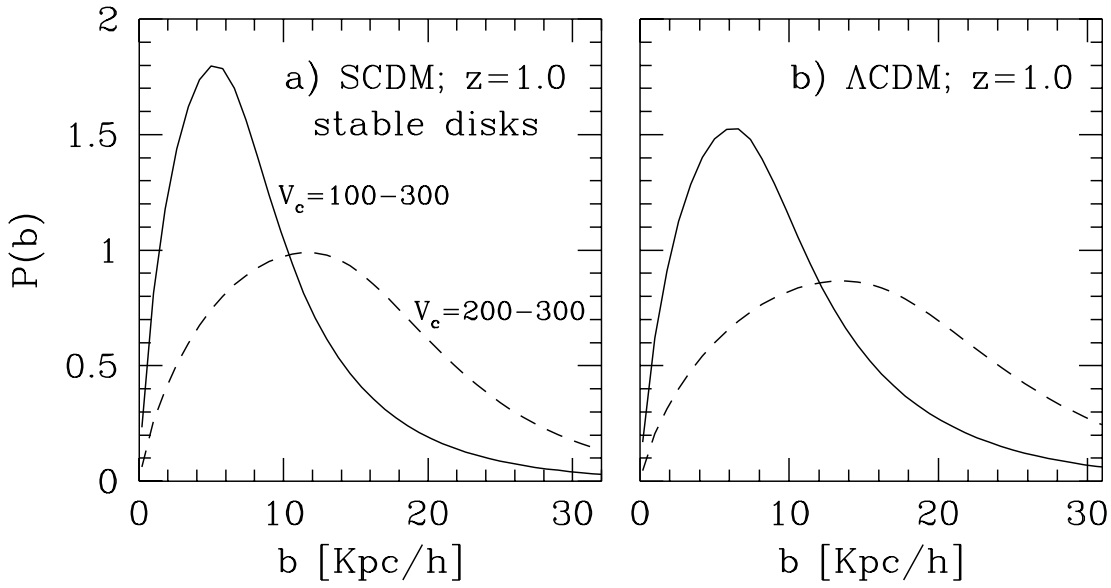


Fig. 12.— The distribution of impact parameter for damped systems in stable disks at $z = 1$. Results are shown for two ranges of $V_c$.

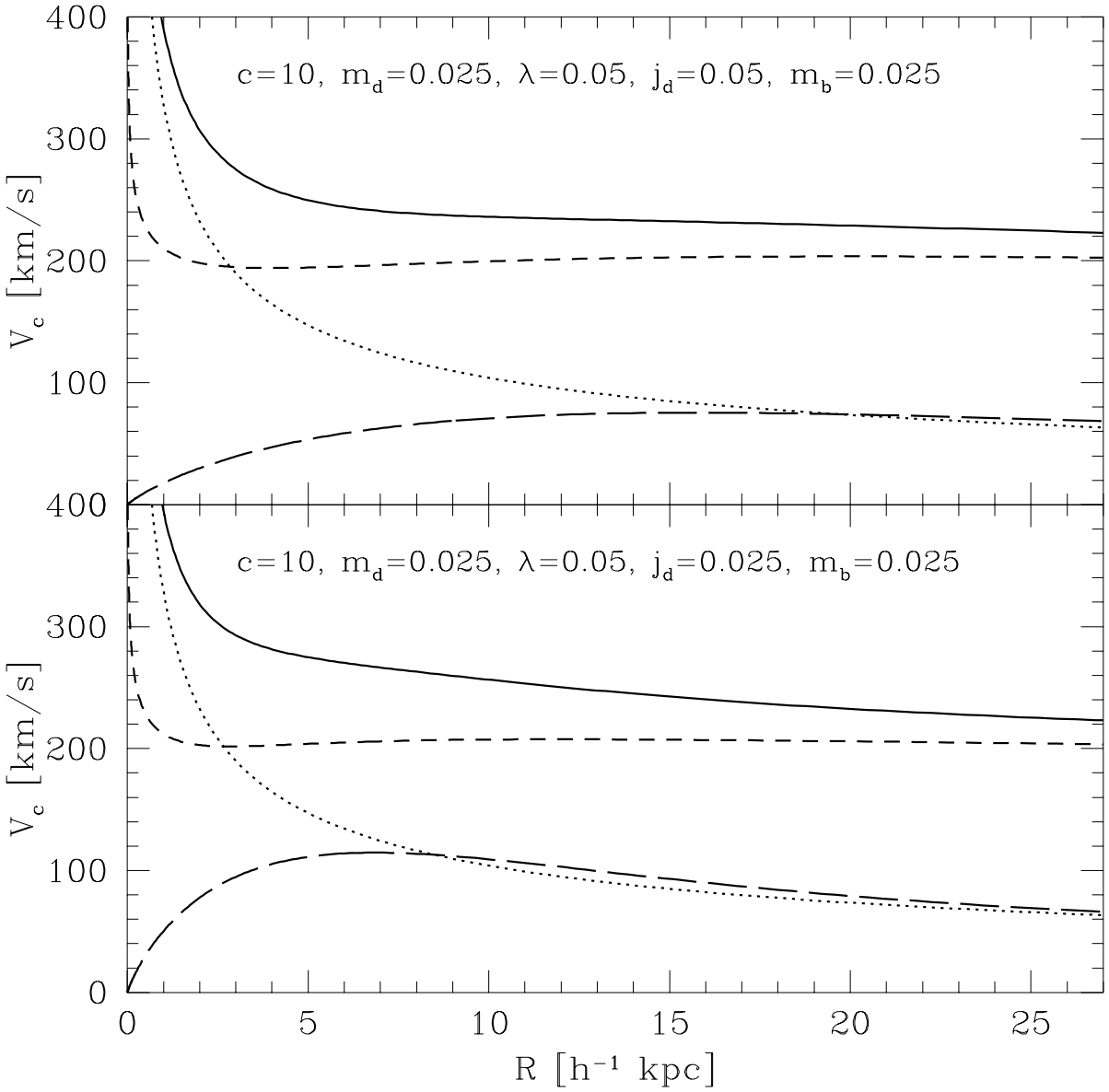


Fig. 13.— Rotation curves for disk galaxies with central bulges (cf. Figure 2). The disk and the bulge are assumed to have the same mass, $2.5 \times 10^{10} h^{-1} M_\odot$. The circular velocities induced by the disk, the bulge and the dark matter are shown by long-dashed, dotted and short-dashed lines, respectively. The total circular velocity is shown by the solid line. In the top panel, the disk is assumed to have twice as much specific angular momentum as the dark matter, while in the bottom panel the two specific angular momenta are assumed to be the same. The central cusps in these rotation curves reflect our unrealistic assumption of a point-mass bulge.

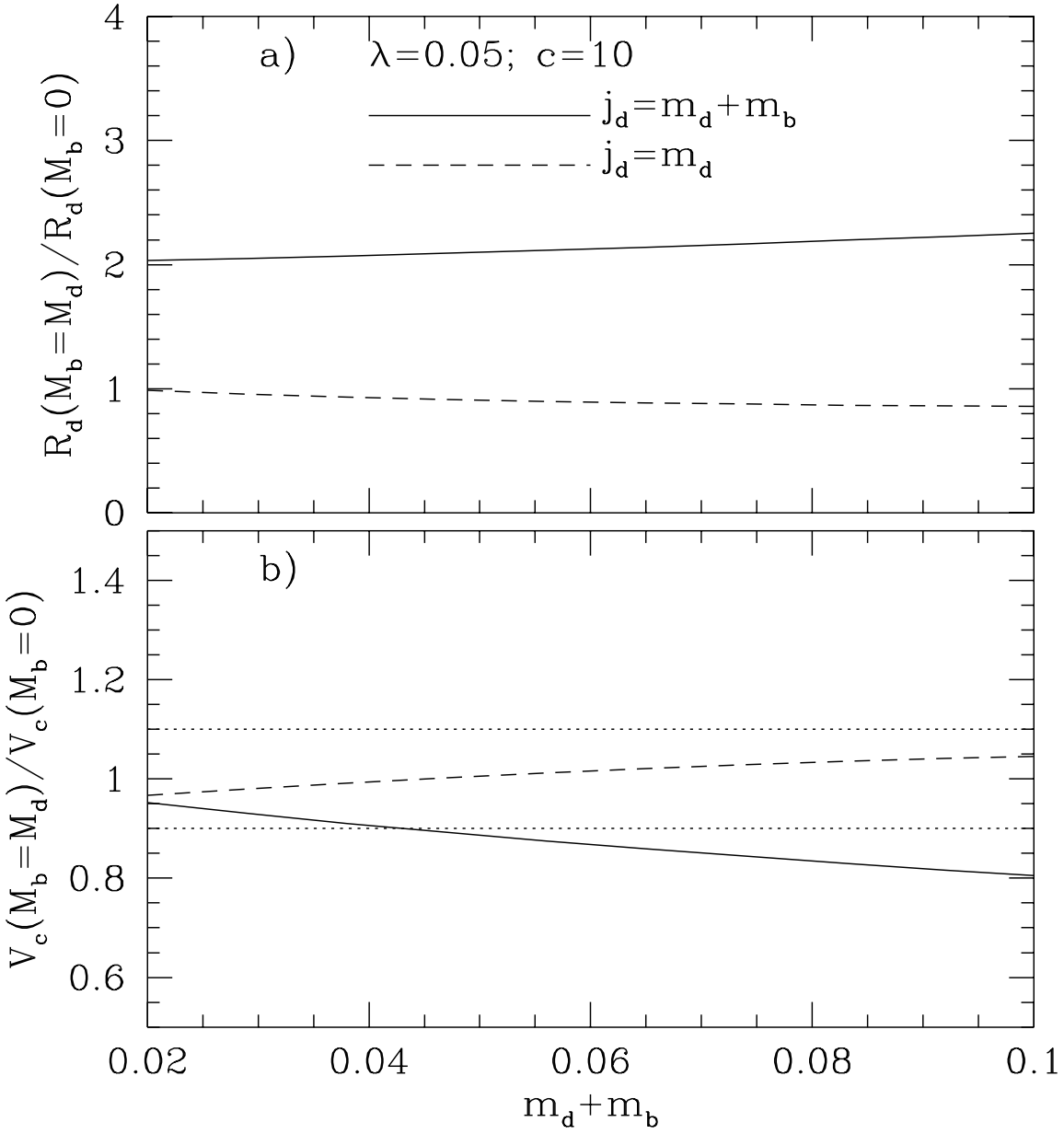


Fig. 14.— Disk scalelength, $R_d$, and disk rotation velocity, $V_c(3R_d)$, in a model where the mass of the central bulge ($M_b$) is equal to that of the disk ($M_d$), as functions of the total stellar mass fraction, $m_d + m_b$. Results are shown in units of the values when $M_b$ is set to zero, We have assumed $\lambda = 0.05$ and $c = 10$. The solid curves show the results for $j_d = m_d + m_b$, while the dashed curves show those for $j_d = m_d$. The two dotted lines give a rough indication of the scatter in the observed TF relation.